Appendix E–FIB-63 Tests

Table of Contents

List of Figures

List of Tables

1 Introduction

Web splitting cracks (Figure 1) typically form during prestress transfer, or in the days and weeks following transfer. They occur due to tensile stresses that are induced as prestressing forces in the bottom flange are distributed through the cross-section (Figure 2).

Figure 1–Web splitting cracks (enhanced in blue)

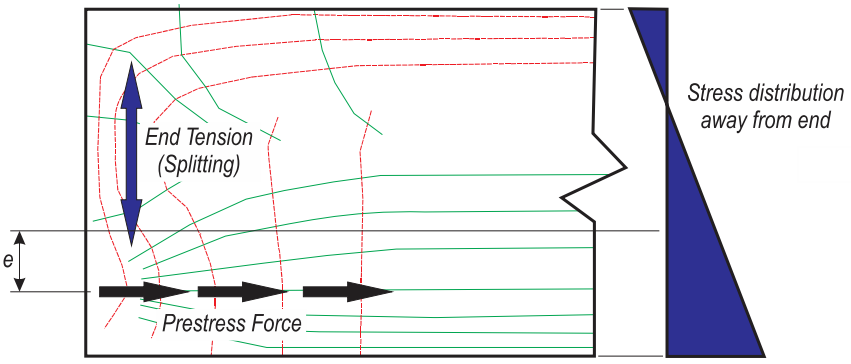

Figure 2–Formation of splitting forces

Some degree of cracking is expected and generally accepted in the end region of pretensioned girders. Indeed, one veteran quality control manager at a precast facility indicated that “My first day on the job I was sent out to monitor web splitting cracks. Years later that’s what I’m still doing.” Web-splitting cracks have also received a good deal of attention in the

research literature, much of which is summarized in Appendix A. Previous research has focused on the causes, design models, reject/repair criteria, and controlling of web-splitting cracks. The current research adds to the body of knowledge by comparing various methods for controlling and/or preventing web splitting cracks. Methods in the current study include: traditional vertical reinforcement, large diameter vertical reinforcement, vertical post-tensioning, and 45% partial strand shielding.

While some cracking is expected, it is also generally accepted that if the cracking is not excessive, then it will not typically impair the girder capacity. It does, however, present serviceability and service life problems. This is particularly true for bridges over salt water. Consequently, this portion of the research project is focused on evaluating methods that may eliminate or reduce this end cracking.

Vertical end zone reinforcement for controlling web splitting cracks is required by AASHTO LRFD Bridge Design Specification (hereafter "LRFD") section5.10.10 (2007). Note that in LRFD 2007, web splitting is referred to as "bursting." Section 5.10.10 requires that vertical reinforcement be placed in pretensioned anchorage zones in sufficient quantity to resist 4% of the prestressing force at transfer ($0.04*P_u$). Stress is limited to 20 ksi and it is placed as close to the end as practicable. These requirements are to be applied at the service limit state.

FDOT has additional requirements for end zone reinforcement beyond those in AASHTO LRFD. Section 4.3.1.D of the FDOT Structures Design Guidelines requires that end zone reinforcement be placed to carry the forces listed below:

- 3% P_u from the end of the beam to h/8, but not less than 10 in.
- 5% P_u from the end of the beam to h/4, but not less than 10 in.
- 6% P_u from the end of the beam to 3h/8, but not less than 10 in.

This requirement is to reduce crack sizes.

2 Test Specimen Design and Construction

Two 63-in. deep Florida I-Beam (FIB-63) girders were fabricated and tested to evaluate the effects of end region detailing on web splitting and ultimate capacity. Each end of each girder was uniquely detailed and is referred to in this document as a distinct specimen. This section presents specimen details, construction procedures, and material properties. The labeling convention used to identify specimens is also presented

2.1 Descriptions and Labels

Four specimens were fabricated, each with different end region details (Figure 3). Specimen CT served as the control specimen and followed current Florida Department of Transportation (FDOT) details (2010). Vertical end zone reinforcement in CT consisted of (16) #5 bars placed within 16.5 in. of the member end. Of the (16) bars, (12) per placed within 9.5 in. of the member end. Quantity and placement of these bars complied with the AASHTO LRFD requirements governing web splitting reinforcement.

Specimen SL had the same end region reinforcement as specimen CT. Strands in SL, however, were 45% partially shielded. Because they were partially debonded, concrete stress associated with transfer length was moved away from the end region. This had the effect of reducing vertical end tension in the web.

LRFD 5.11.4.3 limits the number of shielded strands to 25% of the total number of strands. It also places limits on the number of shielded strands in a row and the number of strands that can have shielding terminate at the same section. Although specimen SL violated these code requirements, it was designed to provide information on the relative effectiveness of strand shielding on limiting web splitting cracks. Specimen SL also allowed for the implications of violating LRFD strand shielding provisions to be evaluated. SL was located on the same girder but at the end opposite of CT.

The end of specimen PT was vertically post-tensioned prior to prestress transfer. The post-tension force was designed to counteract vertical tensile stresses in the web. Vertical reinforcement at the end of PT consisted of the post-tension rods and traditional reinforcing bars. The area of vertical reinforcement was reduced by 33% relative to CT. The post-tension concept used in specimen PT was proposed by the FDOT Structures Design Office.

The fourth and final specimen, LB, had 1-in. diameter threaded rods as vertical end reinforcement. Because it used larger reinforcement, LB had 30% more end reinforcement than CT. Specimen LB was located on the same girder but opposite end as specimen PT.

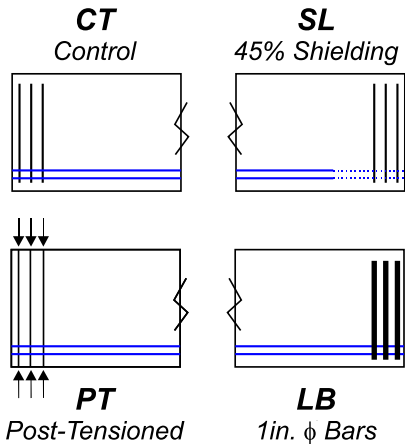

Figure 3–Test specimen labels

2.2 Design

FIB-63 specimens were constructed at the same time and in the same bed as the FIB-54 test girders, which were used in elsewhere in this project (Figure 4) (Appendix D). Since the FIB-54 girders were the primary test specimens in this project, their design dictated strand size, placement, and quantity.

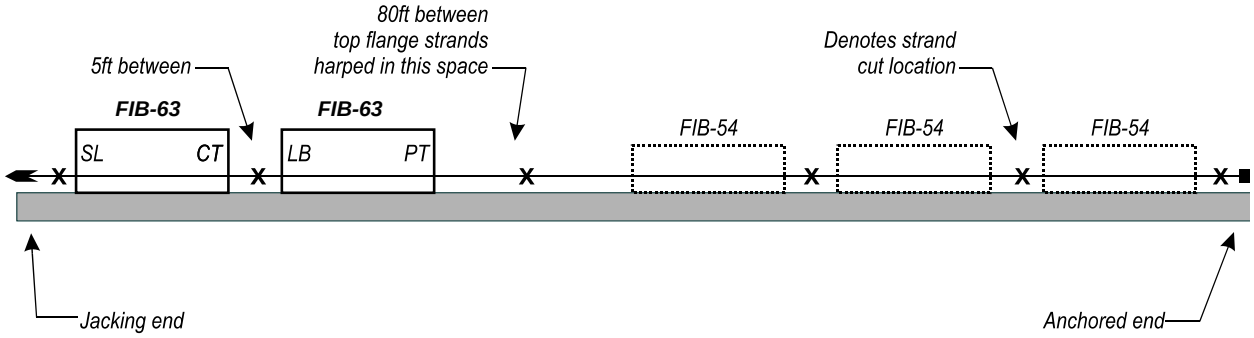

Figure 4–Specimen orientation in stressing bed

Test specimens used the FIB-63 cross-section (Figure 5) and had a total length of 49 ft-6 in. This length was selected to facilitate transport and load testing. Production girders with the same cross-section typically have span lengths over 125 ft.

Specimens had (52) 0.6-in. diameter prestressing strands in the bottom flange and (4) 3/8-in. diameter strands in the top flange (Figure 6). Strands in specimens CT, PT, and LB were fully bonded, whereas strands in SL were 45% partially shielded (Figure 7). The "checker board" shielding pattern used in SL was based on FDOT specifications that prohibit shielding of adjacent strands. As discussed in the previous section, the shielding pattern for SL violated strand shielding provisions of LRFD.

Calculated and allowable longitudinal stresses due to prestressing and self-weight are shown in Figure 8 for the girder with specimens PT and LB. Allowable stresses were calculated according to FDOT and AASHTO LRFD requirements. Specimen CT had the same calculated stresses as those shown in the figure. As demonstrated by Figure 8, specimens CT, PT, and LB exceeded the allowable stress limits in tension and compression. This was intentional to ensure that cracks formed within the end region and to test the detailing schemes under extreme conditions.

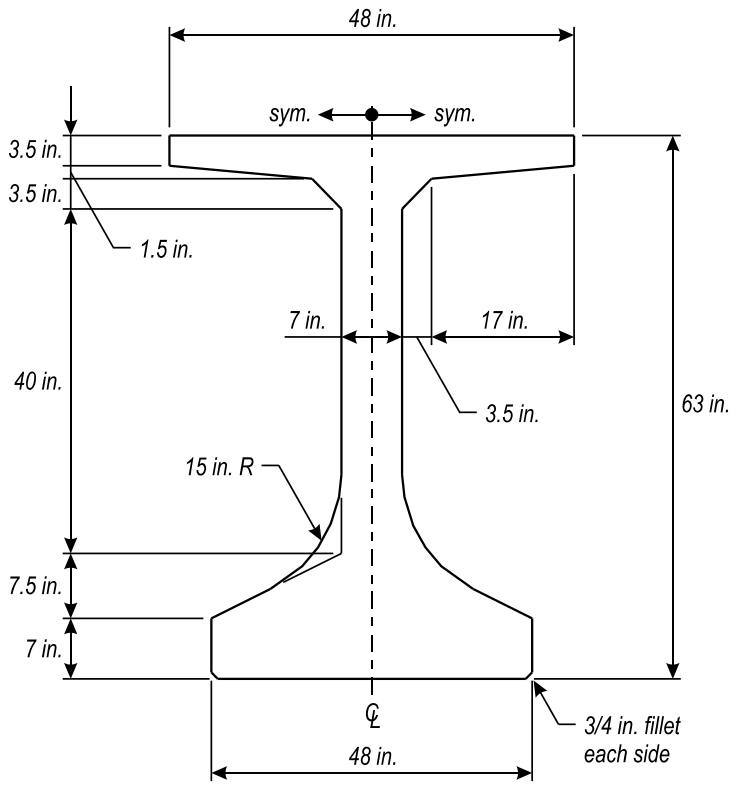

Figure 5–Cross-section FIB-63

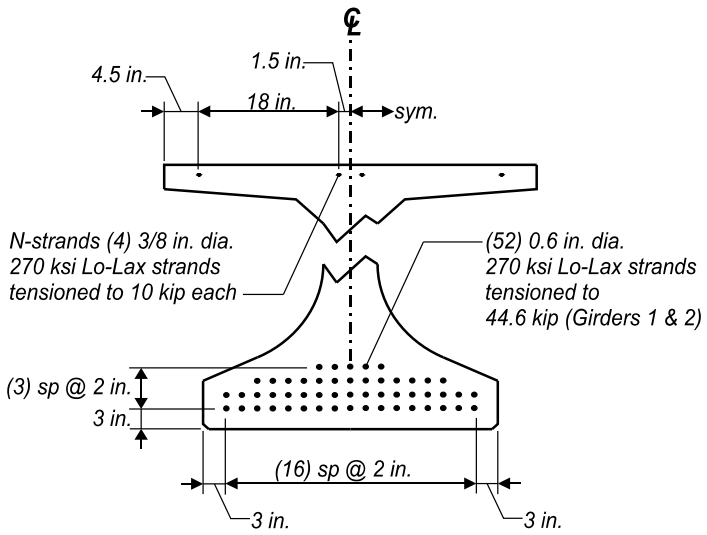

Figure 6–Strand layout and prestressing details

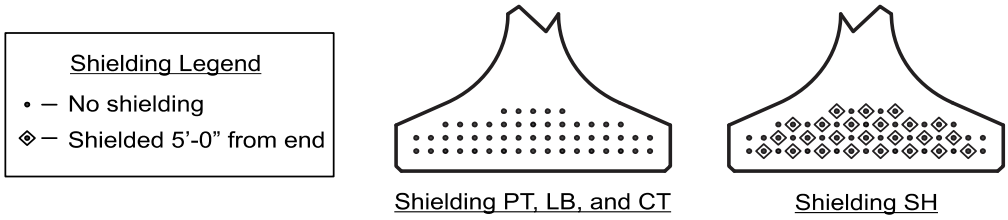

Figure 7–Strand bond and shielding patterns

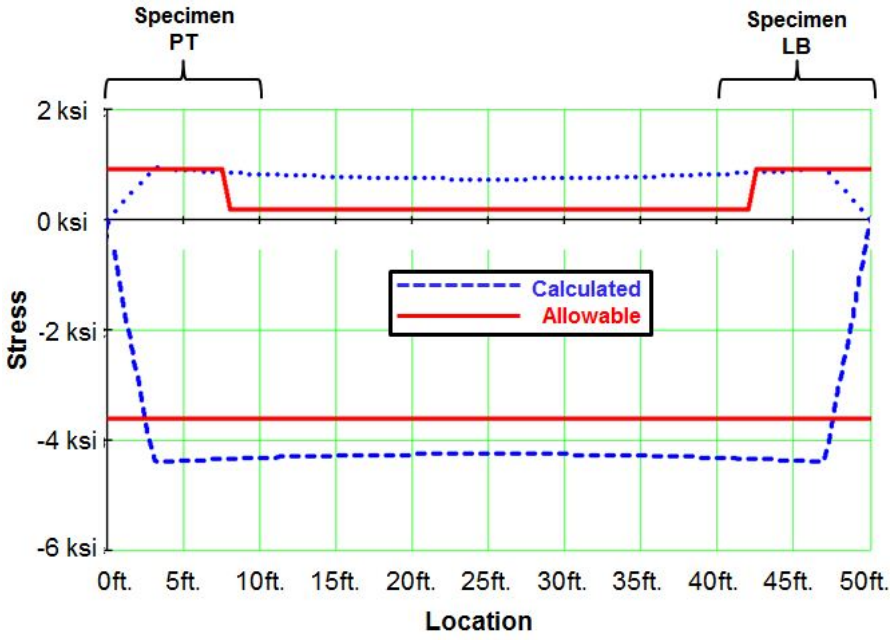

Figure 8–Longitudinal stress due to prestress and self-weight

Mild reinforcement in each specimen (Figure 10 and Figure 11) was based on FDOT FIB-63 Interim Standard Details (FDOT, 2010). Bar labels used in Figure 10 and Figure 11 are typically the same as those used in the FDOT standards. The numeric portion of each label indicates the size of bar (i.e. 5A is a #5 bar). Reinforcement bending and bearing plates details are shown in Figure 11.

Reinforcement labels 8G, 5R, 5Rs, 5T, 5Yt, and 8Y were unique to the test program and are not used in FDOT standards. Unique labels were used to distinguish bars in the FIB-63 girders from bars used in the FIB-54 girders that were fabricated simultaneously. Descriptions of the unique bars are given in the paragraphs below. Descriptions of typical bars are given in Appendix D.

8G. Bars placed longitudinally in the top flange. These bars were included to control cracking in the top flange after prestress transfer, and are not specified in FDOT standards. The G bars did not extend into the end regions where load testing and crack monitoring took place.

5R and 5Rs. Bars placed vertically in the web with hooks top and bottom. These bars were intended to act as shear reinforcement. In production beams these bars have a K label and protruded through the top flange to help develop composite action with the cast-in-place deck. Because a deck was not poured on the test girders, top hooks were embedded in the top flange.

The bottom hook on 5R bars was 16-in. long to assist in constructability. The bottom hook on 5Rs bars was 6-in. long. To eliminate any incidental confinement effects from the bottom hooks, 5Rs bars were used in lieu of 5R bars within the end region.

5T. Bars bundled with 5Rs bars at girder ends. These bars were used to control web splitting cracks.

5Yt. All-thread rods used to post-tension the end of specimen PT. These rods were placed inside of PVC pipes that acted as post-tensioning ducts.

8Y. Vertical all-thread rods placed at the end of specimen LB to control web splitting cracks. Heavy nuts were placed top and bottom to assist in development.

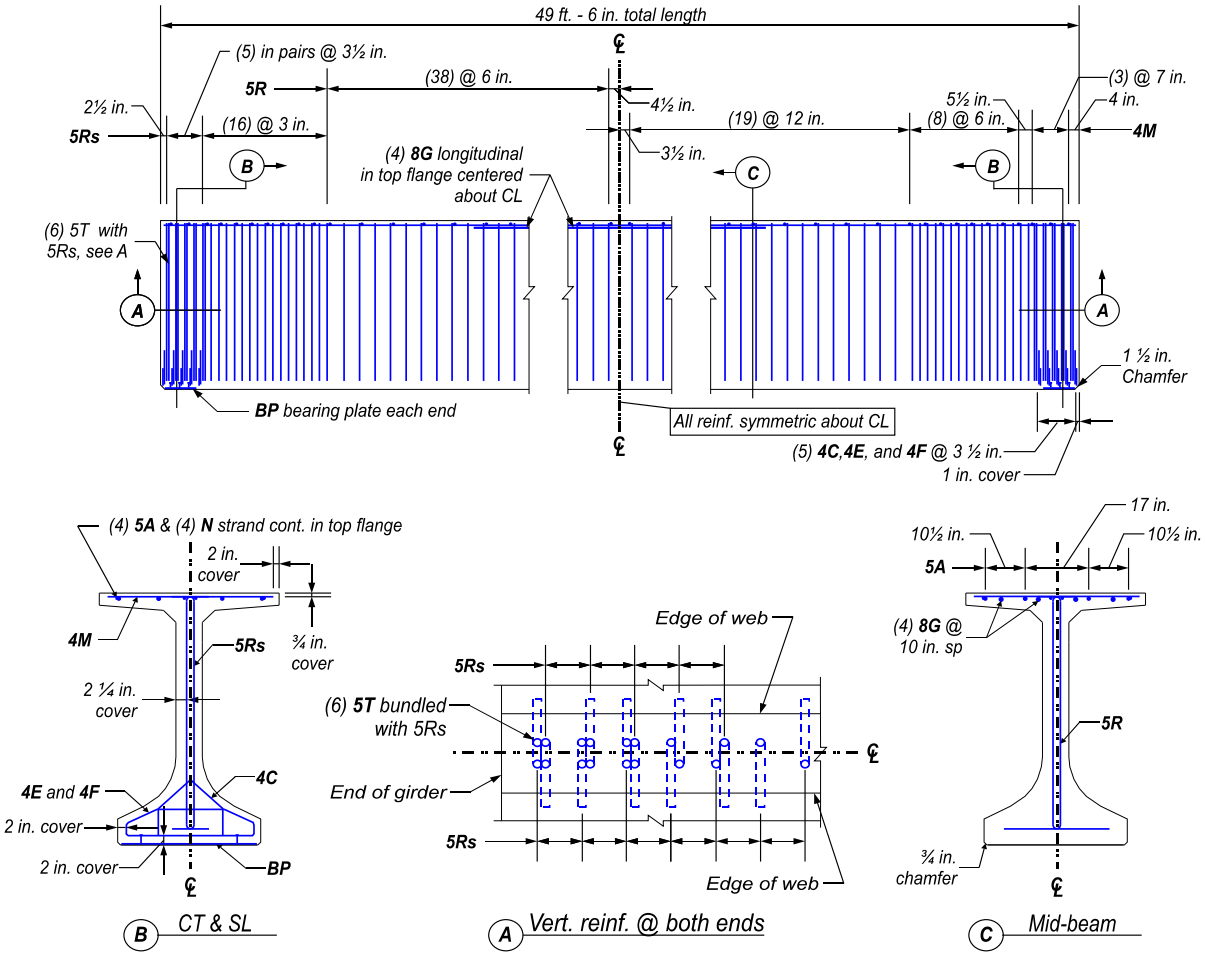

Figure 9–Reinforcement for specimens CT and SL

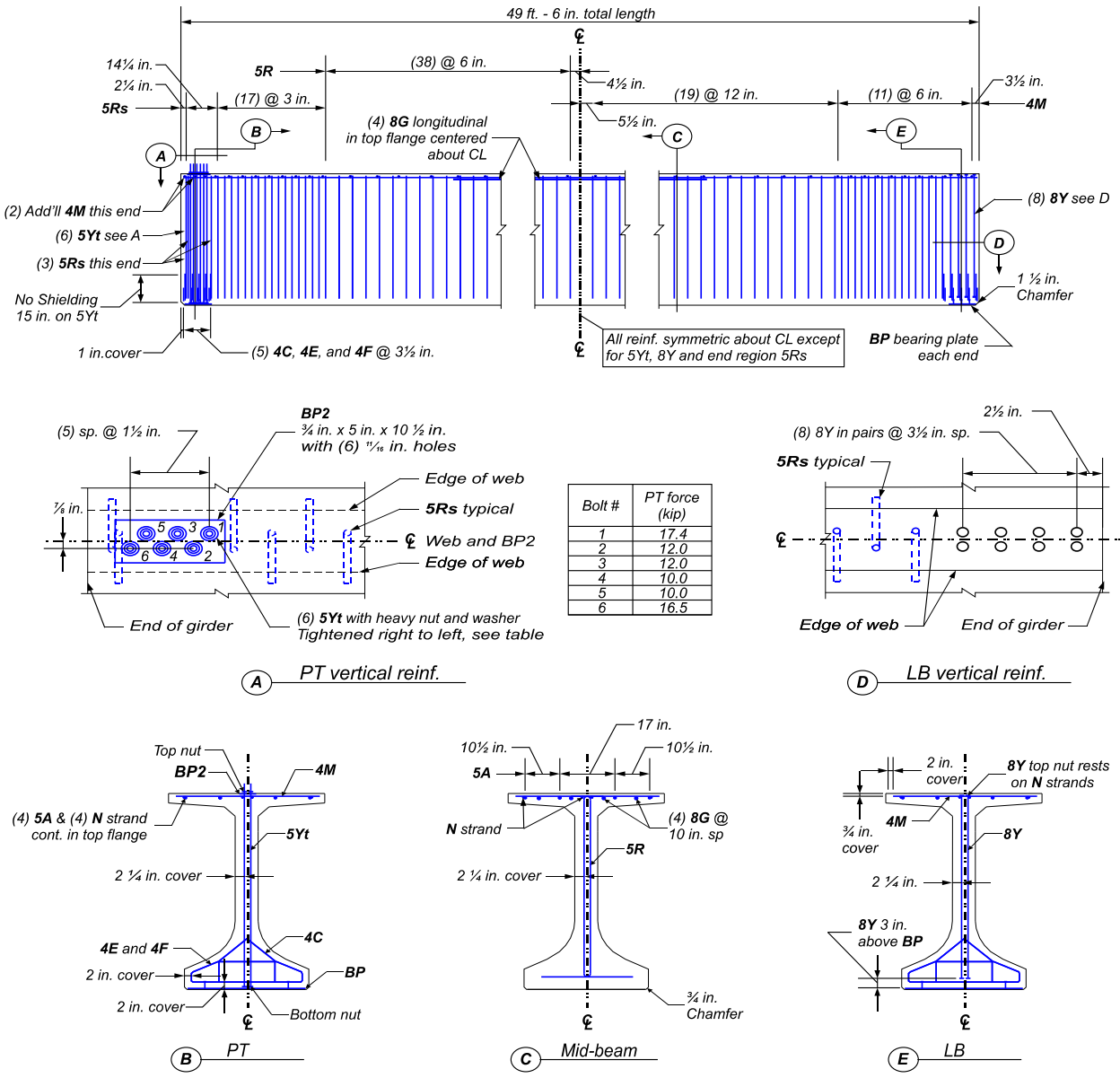

Figure 10–Reinforcement for specimens PT and LB

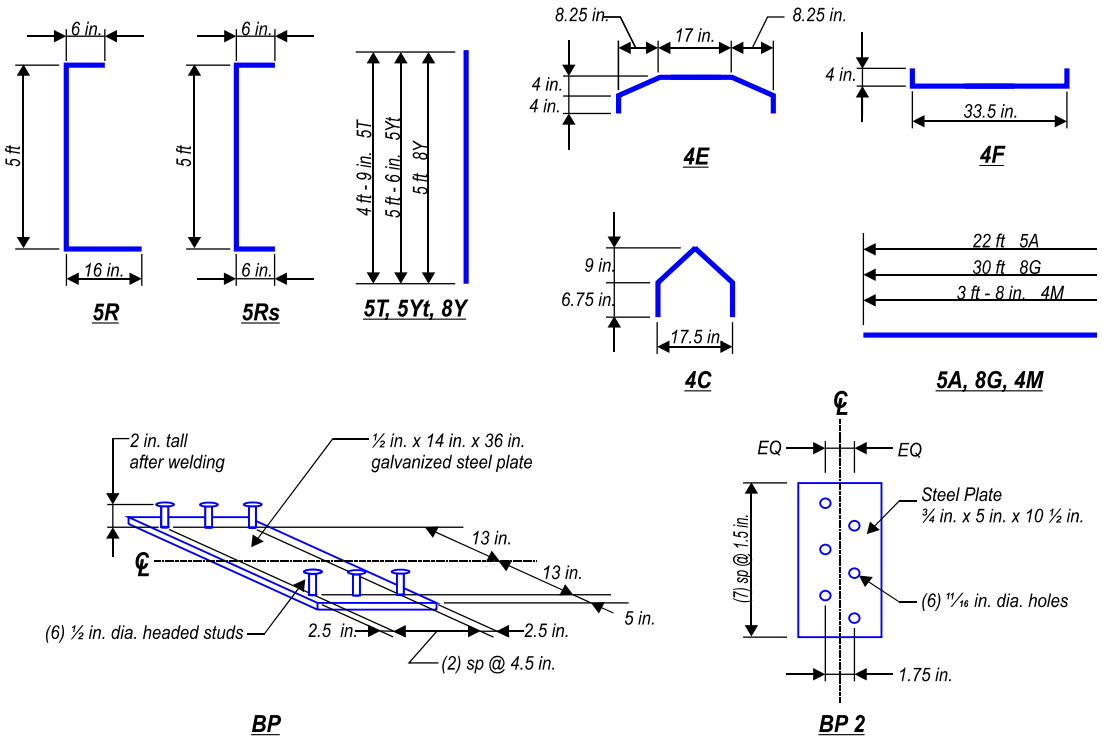

Figure 11–Reinforcement and bearing plate details

Specimens CT and SL both had (16) #5 vertical bars placed within 16.5 in. of the end. Of these bars, (12) were placed within 9.5 in. of the end. Vertical reinforcement in CT and SL satisfied the AASHTO LRFD requirements.

Specimen LB had (8) 1-in. diameter all-thread rods as vertical reinforcement in lieu of the FDOT specified #5 bars. Heavy nuts were placed at the top and bottom of each rod to aid in development, and were necessary because the test specimen did not have sufficient space for standard hooks of #8 bars. In other words, the all-thread rods with nuts allowed development of 1-in. diameter vertical reinforcement where development of hooked bars was not possible. The area of vertical reinforcement at the end of specimen LB was 30% greater than the reinforcement in specimens CT and SL.

Vertical reinforcement at the end of specimen PT also varied from the FDOT standard. In lieu of the standard #5 bars specimen PT had (6) 5/8-in. diameter post-tensioned all-thread rods. PVC pipes were used as post-tensioning ducts in the web. The PVC stopped 15 in. above the bearing plate to allow for development of the rods. To further aid in development, heavy nuts were placed at the bottom of each rod. The top of the rods passed through a 3/4in. thick

steel plate, which served as a bearing plate for the post-tensioning force. Post-tensioning sequence and forces are shown in Figure 10. Grout was not placed in the PVC pipes.

Detailing of the confinement reinforcement in each specimen was modified from the FDOT standard. The modified confinement reinforcement detail used #4 bars in lieu of the FDOT specified #3 bars. Additionally, all confinement bars were placed directly over the bearing in the modified scheme. The modified confinement reinforcement scheme was used for convenience, as it matched the FIB-54 girders that were built simultaneously.

The test FIB-63 specimens were designed for testing without cast-in-place decks. The decision to test without decks was made because it was believed that decks would increase shear capacity of the specimens beyond the capabilities of the available load test equipment. Because decks were not used, vertical reinforcement was developed using hooks in the top flange. The top flange did not provide code-specified cover requirements for the hooks, but was the best possible solution given the test equipment and fabrication constraints.

Specified material properties matched FDOT standards. Specifications are listed in Table 1. Tested material properties will be discussed in a later section.

Table 1–Specified material properties

Material	**Specification**
Girder Concrete	FDOT class VI 8500 psi 28-day compressive strength 6000 psi compressive strength at prestress transfer
Prestressing Strand	ASTM A416 270 ksi ultimate strength Low relaxation
Mild Reinforcement	ASTM A615 60 ksi yield strength
All-thread rods (specimens LB and PT)	ASTM A193 Grade B7

2.3 Construction

Specimens were constructed at Standard Concrete Products in Tampa, FL in February 2012. A time line of construction events is provided in Table 2. Construction began with tensioning of the prestressing strands followed by placement of steel bulkheads. Plastic tubes for strand shielding were placed on the strands prior to tensioning. A hydraulic jack was used to

tension the strands. Jacking force was determined from pressure in the hydraulic line and was verified periodically by measuring strand elongation. Dormant strands in the top flange were tensioned first followed by strands in the bottom flange, which were stressed from the bottom-to-top and outside-in (Figure 13).

Table 2–Fabrication chronology

Event	Phase 2 Date
Strands tensioned	February 13, 2012
Concrete poured	February 17, 2012
Concrete exceeds release strength	February 20, 2012
Forms removed	February 20, 2012
Specimen PT post-tensioned	February 21, 2012
Prestress released	February 21, 2012
Moved to storage	February 22, 2012
Trucked to FDOT laboratory	June 1, 2012
Load testing	June 5, 2012 to June 13, 2012

Figure 12–Jacking frame (left), and steel bulkhead (right).

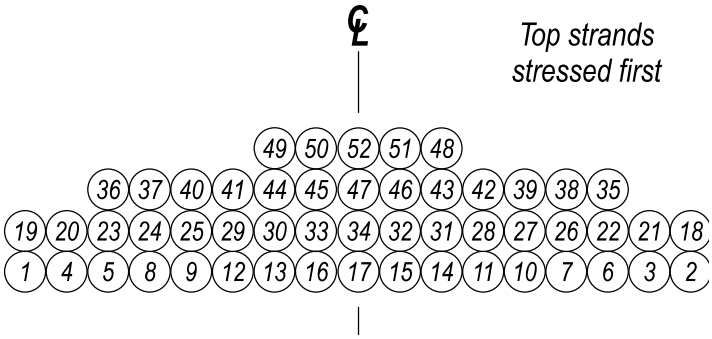

Figure 13–Tension pattern

After tensioning, mild steel reinforcement was placed in each specimen. Select bars were instrumented with strain gages prior to placement in the girders. Figure 14 to Figure 17 show the reinforcement in each specimen. Diagonal strands shown in the web in the pictures are from the lifting loops. Close-ups of the post-tensioning system used in specimen PT are shown in Figure 18. As shown in Figure 18 pipes were placed at the top of two rods to act as spacers for load cells. Close-ups of the 1-in. diameter vertical bars in specimen LB are shown in Figure 19.

Figure 14–Specimen CT reinforcement

Figure 15–Specimen SL reinforcement

Figure 16–Specimen PT reinforcement

Figure 17–Specimen LB reinforcement

Figure 18–Top (left) and bottom (right) of post-tension rods in specimen PT

Figure 19–Top (left) and bottom (right) of all-thread rods in specimen LB

Once reinforcement and internal instrumentation were installed and checked, steel forms were oiled, placed, and squared (Figure 20 and Figure 21). Concrete was mixed at an on-site batch plant and was transported and poured using the fabricator's mix truck and delivery equipment (Figure 22). A self-consolidating concrete mix was used and vibration was not necessary. One batch of concrete was used for both FIB-63 test girders. Concrete test cylinders were taken by the fabricators and by the research team. The top surface of each FIB-63 girder was trowel smooth (Figure 23). Girders were covered with heavy tarps during curing (Figure 23).

Figure 20–Form placement

Figure 21–Form release application (left) and form cross-ties (right)

Figure 22–Concrete delivery (left) and placement (right)

Figure 23–Top flange finish (left) and tarp covers (right)

Forms were removed three days after casting and prestress force was transferred to the girders the day after form removal. The time between form removal and prestress transfer was

used to install surface-bonded foil strain gages, connect the data acquisition system, and apply post-tensioning to specimen PT.

Two 4x8 field cured cylinders were tested on the day of prestress transfer. The average compressive strength was 7320 psi, which was greater than the specified release strength of 6500 psi.

Specimen PT was post-tensioned a few hours prior to prestress transfer (Figure 24). The post-tensioning force was applied by hand using a socket wrench. A pipe was placed over the wrench to increase leverage. Even with the increased leverage the process required the strength of two men.

Rods were tensioned sequentially starting with the rod farthest from the end, and finishing with the rod closest to the end (Figure 10). Load cells were used to monitor force in the first and final rods during post-tensioning. Forces in the other rods were estimated using the turn-of-the-nut method. Turn-of-the-nut estimations were calibrated using data from the load cells and from linear-elastic mechanics principles. Load cell data were particularly helpful in determining the number of turns beyond snug-tight that were required to engage the rods. Measured and estimated loads are shown in Figure 10 and listed in Table 3.

Forces in the individual rods were influenced by the relative difficulty of the post-tensioning process. In spite of these difficulties a total post-tensioning force of 77.9 kip was obtained. This value is within the acceptable range as determined from preliminary analysis conducted prior to fabrication. The total applied post-tension force was approximately 3.4% of the initial pretension forces.

Figure 24–Post-tensioning specimen PT (left) and load cells and anchor plate (right)

Table 3–Post-tensioning force measured in specimen PT

Rod number (corresponds to stressing sequence)	Post-tension force (kip)	Measurement method
1 (farthest from end)	17.4	Load cell
2	12.0	Turn-on-the-nut
3	12.0	Turn-on-the-nut
4	10.0	Turn-on-the-nut
5	10.0	Turn-on-the-nut
6 (closest to end)	16.5	Load cell
Total	77.9	

Flame cutting was used to release the prestressing strands. Individual strands were cut simultaneously at points shown in Figure 4. Dormant strands in the top flange were cut first, followed by the bottom strands, which were cut from the outside-in and from bottom-to-top (Figure 25). This release pattern was selected because it is relatively easy to execute and because it is typical of precast girders in Florida. Strand cutting was stopped intermittently at multiple stages to obtain strain readings from vibrating wire strain gages and to check for cracking.

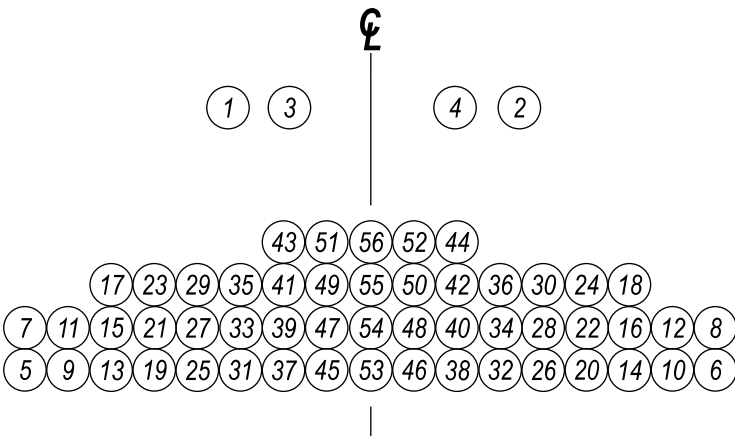

Figure 25–Strand cutting pattern

The girders shifted slightly (less than 1 in.) along the length of the stressing bed multiple times during prestress transfer. Movement events always corresponded to strand cuts.

Girders were moved from the stressing bed to storage yard the day after prestress was transfer (Figure 26). While in storage the girders were examined periodically for cracking. After three months in storage girders were trucked (Figure 27) to the Marcus H. Ansely FDOT structures laboratory in Tallahassee, FL for load testing.

Figure 26–Girder lifted by crane

Figure 27–Test girder transported by truck

2.4 Material Properties

Concrete, mild steel, and prestressing strand were selected to match FDOT specifications. FDOT class VI concrete (f'c = 8500 psi) was specified for the girders. Concrete compressive strength was tested using both 4x8 and 6x12 cylinders. Table 4 presents the tested concrete strengths.

Prestressing strands were Grade 270 low-relaxation, conforming to ASTM A416. Tested strand properties are shown in Table 5.

Bond capacity of the prestressing strands was tested in accordance with the proposed standard recommended by the North American Strand Producers (NASP 2009). Table 6 lists results of the NASP tests.

Table 7 presents the tested material properties for mild steel reinforcement. All reinforcement was ASTM A615 grade 60.

Table 4–Tested concrete compressive strengths

Material	Cast date	Test date	Average strength (psi)	Sample size	Testing agent*	Cure Method
Phase 2 Girder Concrete	2-17-12	2-20-12	7050	(2) 4x8 cylinders	1	Wet
		2-21-12	7330	(2) 4x8 cylinders	1	Field
		3-02-12	8790	(2) 4x8 cylinders	1	Wet
		3-16-12	8250	(3) 6x12 cylinders	2	Wet
		3-16-12	9210	(3) 4x8 cylinders	1	Wet
		5-30-12	10,520	(3) 6x12 cylinders	3	Field

* 1. Tested by girder fabricator
2. Tested by FDOT State Materials Office
3. Tested by FDOT Structures Research Center

Table 5–Prestressing steel properties

Material	Stress at 1% elongation	Ultimate stress	Elongation at ultimate stress	Testing agent*
Prestressing Strand	261 ksi	287 ksi	5.38%	1
	259 ksi	285 ksi	NA	2

* 1. Strand supplier
2. FDOT State Materials Office (average of 4 samples)

Table 6–NASP test results

Test Number	Load at 0.1-in. strand slip (lb)
1	26400
2	21600
3	23400
4	24400
5	21300
6	28200
Average	24200

Table 7–Steel reinforcement properties

Material	Yield Stress	Ultimate Stress	Elongation at Ultimate Stress	Testing agent*
#4 confinement rebar	70.0 ksi	109.1 ksi	11%	1
	76.4 ksi	106.8 ksi	11%	2
#5 vertical rebar	64.5 ksi	103.2 ksi	11%	1
	63.2 ksi	103.5 ksi	13%	2
* 1. Rebar supplier 2. FDOT State Materials Office (average of 2 samples minimum)				

3 Test Procedures

3.1 Fabrication

This section describes the procedures used to collect strain and crack data during fabrication. Data were collected during post-tensioning of specimen PT, during prestress transfer, and while the specimens were in storage awaiting transport.

Specimen PT Post-tensioning. It was assumed that post-tensioning of specimen PT did not affect the other specimens so data were only collect from specimen PT during this process. Prior to applying the post-tensioning, specimen PT was examined for cracks and null readings were taken from all instruments. Data from strain gages were monitored and logged using a computerized data acquisition system powered by portable generators. Data from vibrating wire strain gages were monitored using an electronic readout box and logged manually. The data acquisition systems were placed in a van adjacent to the stressing bed. Cracks were not observed during post-tensioning so no crack data were collected during this phase.

Prestress transfer. Strain and crack data were collected from each specimen during prestress transfer. Prior to transfer girders were examined for cracks and null readings were taken from all instruments. Data from strain gages were monitored and logged using a computerized data acquisition system powered by portable generators. Data from vibrating wire strain gages were monitored using an electronic readout box and logged manually. The data acquisition systems were placed in a van adjacent to the stressing bed. Strand cutting was paused at various times during prestress transfer to allow for visual inspection of the specimens and to take readings from the vibrating wire gages. Visual inspections and vibrating wire readings were also conducted after prestress transfer was complete. Crack locations were marked with a crayon or marker and documented by photograph. Crack widths were measured at few locations using a microscope that was precise to +/- 0.001 in. Crack lengths were determined by visual inspection with the naked eye.

Storage. Specimens received periodic visual inspections while they were in storage at the precast facility. During these inspections cracks were marked then documented by photograph. Crack widths were measured by microscope at few locations on each end region crack. Dates of visual evaluations are listed in Table 8. Vibrating wire gage data were also collected while the girders were in storage.

Table 8–Construction events and inspection dates

Event	Inspection Date	Days after prestress transfer
Form Removal	February 20, 2012	--
Prestress Transfer	February 21, 2012	0
In storage immediately after lifting	February 22, 2012	1
In storage	February 23, 2012	2
In storage	February 24, 2012	3
In storage	March 6, 2012	14
In storage	March 22, 2012	30
In storage	April 9, 2012	48
Prior to load testing	June 1, 2012	101

3.2 Load Testing

Load tests were conducted at the FDOT M. H. Ansley Structures Research Center in Tallahassee, FL. Test dates are listed in Table 9. Load tests were conducted on both ends of each girder. After the first end (specimen) was tested, the supports and load point were moved and the opposite end was tested.

Table 9–Load test chronology

Specimen	Test Date (service and ultimate)
PT	06/06/2012
LB	06/05/2012
CT	06/13/2012
SH	06/11/2012

Each specimen was loaded at least twice. The first loading simulated a service load of approximately 500 kip. Once the service load was reached, the load was held constant and cracks were identified and marked. After the cracks were marked the load was removed. The second loading was intended to determine each specimen's ultimate strength. A load-displacement plot was monitored real-time during the ultimate load test. Load was applied until it was apparent from the load-displacement plot that peak capacity had been reached, or until the capabilities of the test equipment were reached. Cracking was documented after the ultimate load test was complete.

Load and support geometry are shown in Figure 28. Each support consisted of a 10-in. x 32-in. reinforced bearing pad. Pads were "Type E" pads constructed according to FDOT design

interim design standards (FDOT 2009). The bearing pad at the near support was centered below the embedded steel bearing plate (Figure 29).

Load was applied to the specimen using side-by-side hydraulic actuators. The load rate was controlled by adjusting a pump that pressurized the hydraulic system. The combined load rate varied from 0.1 kip/sec to 0.6 kip/sec, with the typical rate being approximately 0.4 kip/sec. Load was spread from the actuators to the girders through steel plates and a 10 in. x 30 in. reinforced neoprene bearing pad. The orientation of the bearing pad and steel plate at the load point for specimen LB is shown in Figure 32. This orientation affected an undesirable failure mode in LB, so the bearing pad and plate orientation were changed for the remaining tests. The modified load point setup oriented the bearing pad parallel with span length of the specimen and placed an additional steel spreader beam to distribute the load (Figure 31). A reaction frame was used to transmit load from the actuators to the strong floor (Figure 32).

Load, displacement, strand slip, and strain data were continuously collected during the service and ultimate load tests. Strain from the vibrating wires strain gages was collected at discrete points during load testing. Concrete samples were tested in conjunction with the load tests to determine compressive strength at the time of load testing.

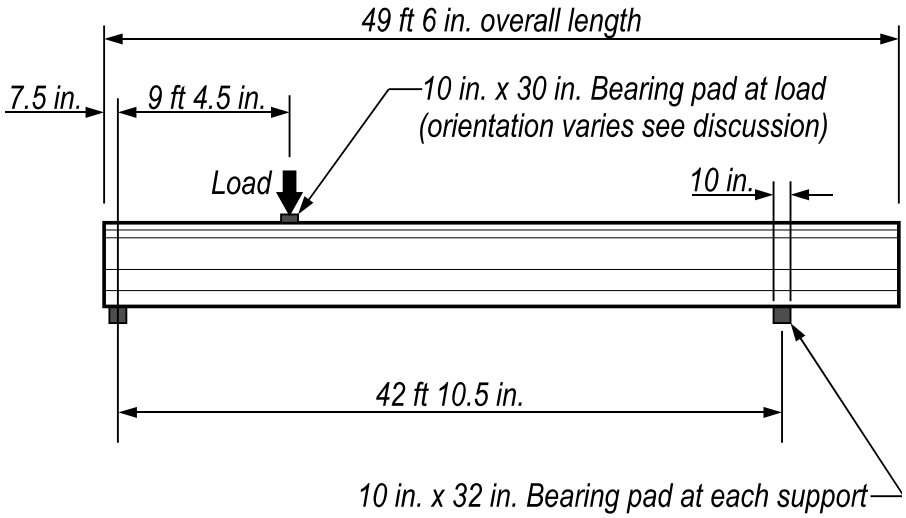

Figure 28–Test setup

Figure 29–Support conditions at bearing

Figure 30–Support conditions at load point for specimen LB

Figure 31–Support conditions at load point for specimens CT, SL, and PT

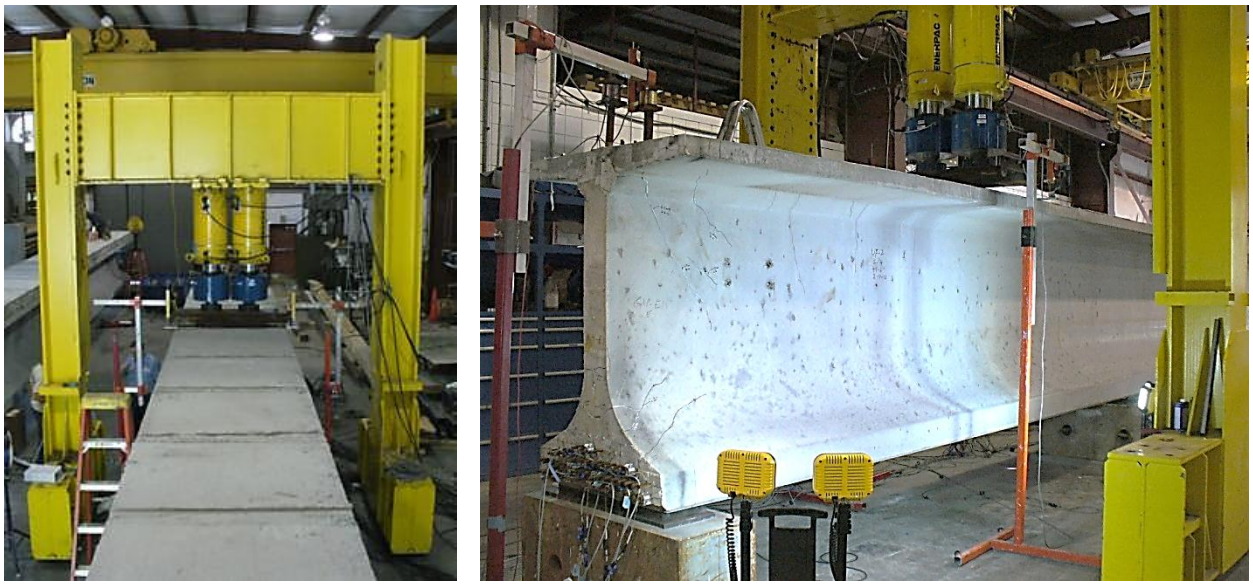

Figure 32–View of test specimen and load frame from above (left)
and side view of specimen (right)

3.3 Coordinate System

A consistent coordinate system is used throughout this document to define instrumentation locations and to identify the direction of strains, stresses, and forces. The origin for the coordinate system is placed at the centerline of the cross-section, at the bottom of the girder, and at the girder end (Figure 33). The z-direction is vertical, the x-direction is horizontal across the width of the girder, and the y-direction is horizontal along the span length. The support nearest the origin is denoted as the near support, and the opposite end is denoted as the far support.

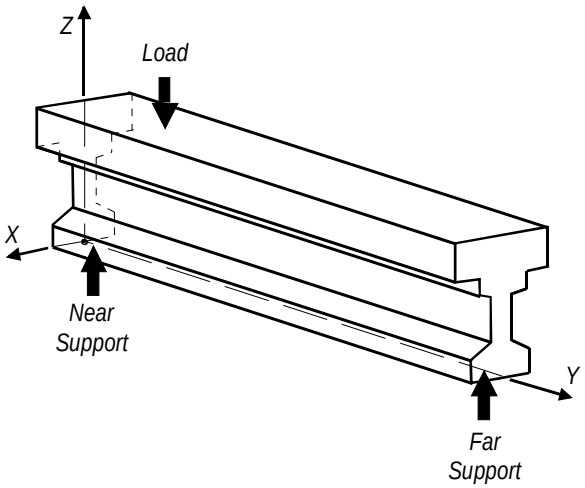

Figure 33–Coordinate system relative to load and supports

4 Instrumentation

Strain, displacement, force, and crack data were collected during fabrication and load testing. This chapter describes the instrumentation used to collect data and the labeling scheme used to identify the various instruments.

4.1 Types and Descriptions

Data were collected using load cells, LVDTs, linear potentiometers, variable resistance strain gages and vibrating wire strain gages. Table 10 lists the different types of instrumentation and the associated labels. With the exception of the vibrating wire strain gages, all data were logged electronically. Vibrating wire gage data were logged manually from an electronic readout box.

Table 10–Instrumentation types and labels

Label	Type	Placement
MS	Foil strain gage	Reinforcement
XS	Foil strain gage	Concrete surface
ES	Embedded strain gage	Concrete interior
V	Vibrating wire strain gage	Concrete interior
S	Foil strain gage	Concrete surface
L	Linear variable displacement transducer (LVDT)	Load point and supports
P	Linear potentiometer	Strands
--	Load Cell	Load point / post-tension rod

MS strain gages were attached to select mild reinforcement prior to placement in the test girders (Figure 34). MS gages had a gage length of 5mm and were used to monitor strain during load testing.

XS strain gages (Figure 35) were attached to the surface of test girders immediately after formwork was removed. These gages were used to measure concrete strains during prestress transfer. XS gages had a 60mm gage length.

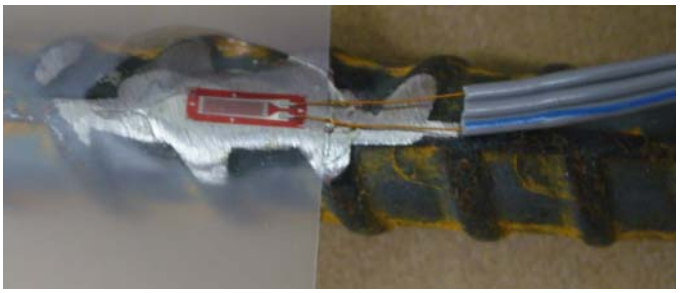
A

B

Figure 34–MS gage installation showing A) gage before protective covering and B) protective cover and label

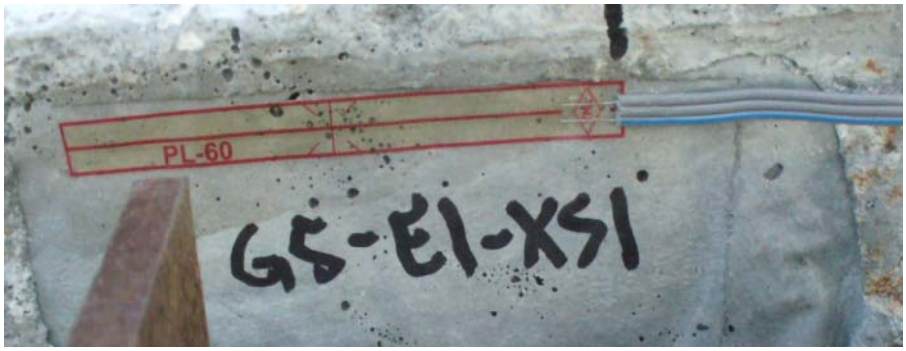

Figure 35–XS gage installation

ES gages were embedded in the test girders and were used to monitor concrete strain during prestress transfer and load testing. ES gages had a gage length of 60mm. Figure 36 shows ES gage installation prior to concrete placement. Wire leads from ES gages were routed along reinforcement and exited from the top flange. A label was placed at the end of each wire lead for identification purposes.

V series gages were vibrating wire strain gages which were embedded in the test girders. These gages had a gage length of 152mm and were used to measure concrete strain during all phases of fabrication and load testing. Figure 37 shows a V series gage installation prior to concrete placement. Because vibrating wire gages do not experience electronic drift over time, they were particularly useful in monitoring prestress losses.

Figure 36–ES gage installation

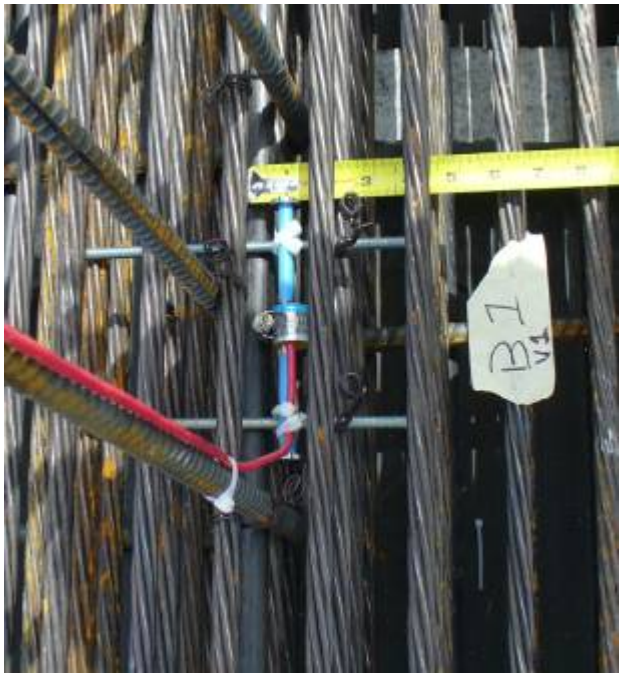

Figure 37–V gage installation (view from above)

S series strain gages were installed at discrete locations on girder surfaces (Figure 38). These gages had 60mm gages lengths and were used to monitor concrete strain during load testing.

L series instruments were LVDTs used to monitor vertical displacement during load tests. Labels and locations of the LVDTs measuring vertical displacement are shown in Figure 39. LVDTs were mounted to fixed support structures as shown in Figure 40.

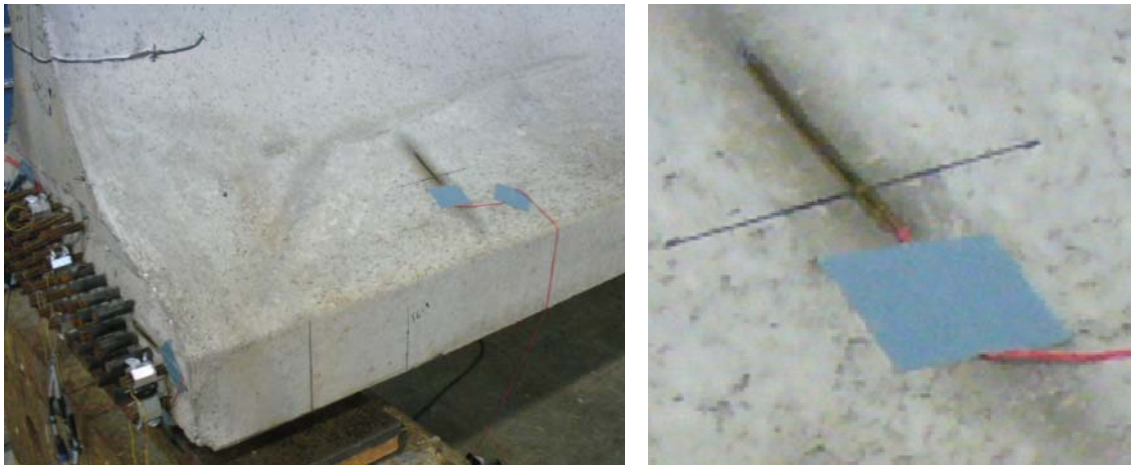

Figure 38–S gage installation on bottom flange (left) and close-up (right)

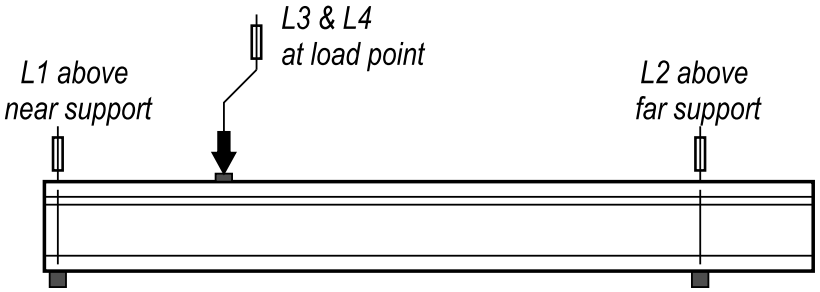

Figure 39–LVDT placement and labels

Figure 40–LVDT and support frame

P series variable resistant potentiometers were used to measure strand slip. Instrumented strands are shown in Figure 41. P series instruments were mounted directly to the strands using custom-machined aluminum brackets and set-screws (Figure 42).

Load cells (Figure 43) were used to measure the force applied during the load tests. A hydraulic system was used to apply the loads, and a pressure transducer was used to measure pressure in the hydraulic line during testing. Both force and pressure data were logged electronically, along with displacement and strain data from the other instruments.

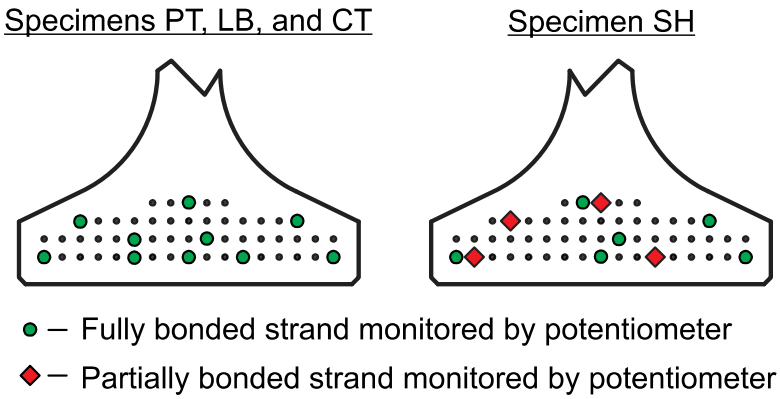

Figure 41–Strands monitored by potentiometers

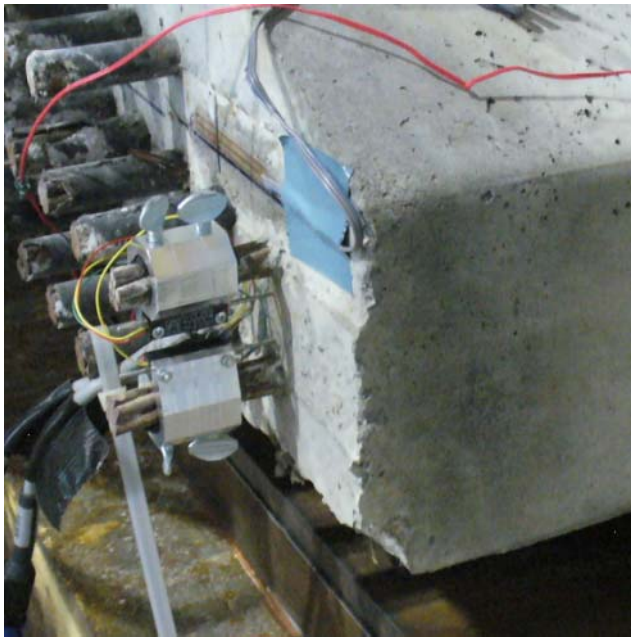

Figure 42–Aluminum brackets and linear potentiometers on strands

Figure 43–Load cells below hydraulic actuators

4.2 Strain Gage Coordinates

Figures in this document presenting strain data typically also contain information regarding the location of gage(s) from which the data were collected. Information in the figures gives a general idea of the gage orientation and position but doesn't always give specific coordinates. Table 11 through Table 14 give specific coordinates of gages referenced in this document. Coordinates are based on the system defined in Figure 33. Many gages used in the experimental program are not specifically referred to in this document.

Table 11–Specimen CT strain gage coordinates

Instrument	X (in.)	Y (in.)	Z (in.)	Orientation	Reference(s)
XS2	3.5	0.5	24	Z	Figure 50
XS3	3.5	4.25	24	Z	Figure 50
XS4	3.5	12	23.5	Z	Figure 50
XS5	19	6	6	Y	Figure 56
XS6	19	12	6	Y	Figure 56
XS7	19	17.5	6.25	Y	Figure 56
XS8	19	24	6.25	Y	Figure 56
XS9	19	29.75	6.25	Y	Figure 56
XS10	19	35.25	6	Y	Figure 56
V2	0	297	7.75	Y	Table 17
S4	3.5	72	36	Y-Z	Table 18

Table 12–Specimen SL strain gage coordinates

Instrument	X (in.)	Y (in.)	Z (in.)	Orientation	Reference(s)
XS2	3.5	0.5	24	Z	Figure 51
XS3	3.5	4.0	24	Z	Figure 51
XS4	3.5	12.0	24	Z	Figure 51
V2	0.0	297.0	7.5	Y	Table 17
S4	3.5	72.0	36.0	Y-Z	Table 18

Table 13–Specimen PT strain gage coordinates

Instrument	X (in.)	Y (in.)	Z (in.)	Orientation	Reference(s)
XS1	1.5	0	62.5	X	Figure 47
XS2	3.5	1.5	24.0	Z	Figure 47, Figure 52
XS3	3.5	4.0	24.0	Z	Figure 47, Figure 52
XS4	3.5	12.0	24.0	Z	Figure 47, Figure 52
V1	0.0	1.5	17.0	Y	Figure 45
V2	0.0	296.0	8.5	Z	Table 17
S4	3.5	72.0	36.0	Y-Z	Table 18

Table 14–Specimen LB strain gage coordinates

Instrument	X (in.)	Y (in.)	Z (in.)	Orientation	Reference(s)
XS2	3.5	0.5	23.5	Z	Figure 53
XS3	3.5	4.0	24.5	Z	Figure 53
XS4	3.5	12.0	23.5	Z	Figure 53
V2	0.0	298.0	8.5	Z	Table 17
S4	3.5	72.0	36.0	Y-Z	Table 18

5 Test Results and Discussion

5.1 Strain during Post-Tensioning

Vertical rods at the end of specimen PT were post-tensioned prior to cutting of the prestressing strands (Figure 10). Strain data from the concrete, as well as force data from the rods were collected during the post-tensioning process. Strain and load data are documented in this section.

Force data are presented in Figure 44 for rods #1 and #6. Time zero in the figure corresponds to the start of the post-tensioning. Rod #1 was farthest from the specimen end and was stressed first. Rod #6 was closest to the end as was stressed last. Tension in rod #1 reached a peak of 18 kip. At the end of post-tensioning the tension in #1 had reduced to 17.4kip. Loss of tension is the result of elastic losses as the other rods were being tensioned. Tension in #6 was 16.5 kip at the end of the post-tensioning process. Elastic losses did not affect rod #6 as it was the last rod to be tensioned.

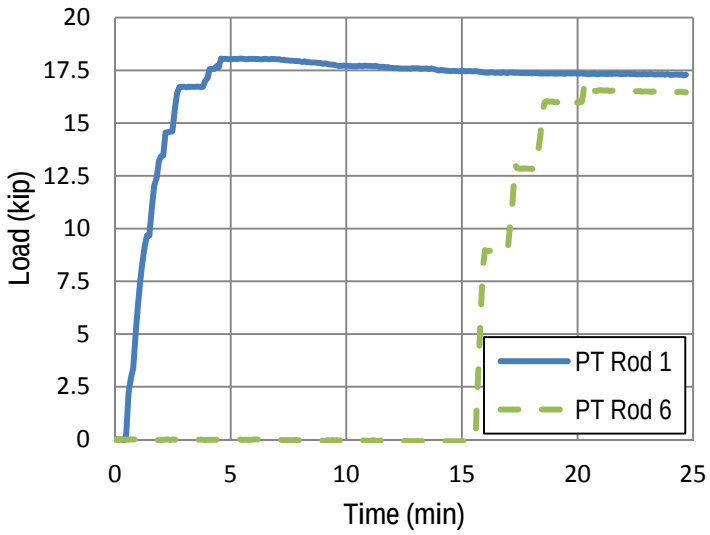

Figure 44–Variation in load during post-tensioning process

Tension in rods #2 though #5 were estimated using the turn-of-the-nut method. Tension force resulting from each turn was calibrated using data from rods #1 and #6 and was verified using linear elastic analysis of the rod elongation. The total post-tension force was estimated to

be 78kip. Dividing this number by the total number of turns suggests that post-tensioning was applied at a rate of approximately 6 kip/turn.

Strain effects from each turn-of-the nut are plotted in Figure 45. Strain in Figure 45 is from the vibrating wire gage placed vertically in the bottom flange (Figure 46). Strain at this location increased as the cumulative number of turns increased throughout the post-tensioning process. Abrupt jumps in the data at 2.2 turns and at 6.5 turns occurred during pauses in the post-tensioning. The strain-per-turn rate increased towards the end of the process as rods closer to the vibrating wire gage were tensioned.

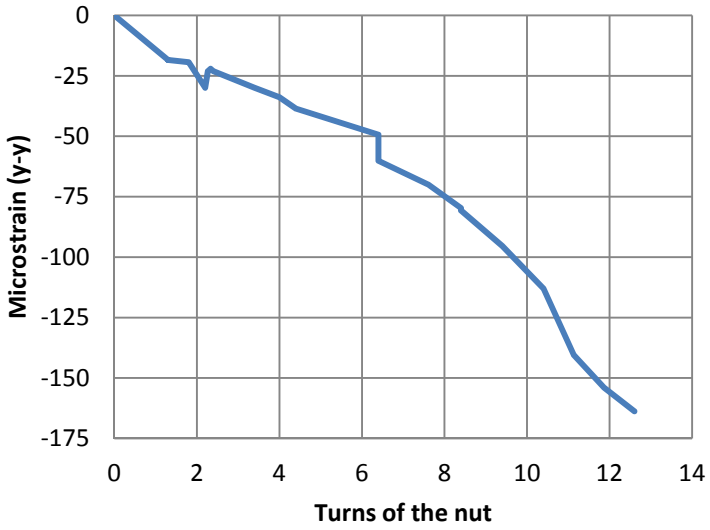

Figure 45–Strain measured by V1 gage during the post-tensioning process

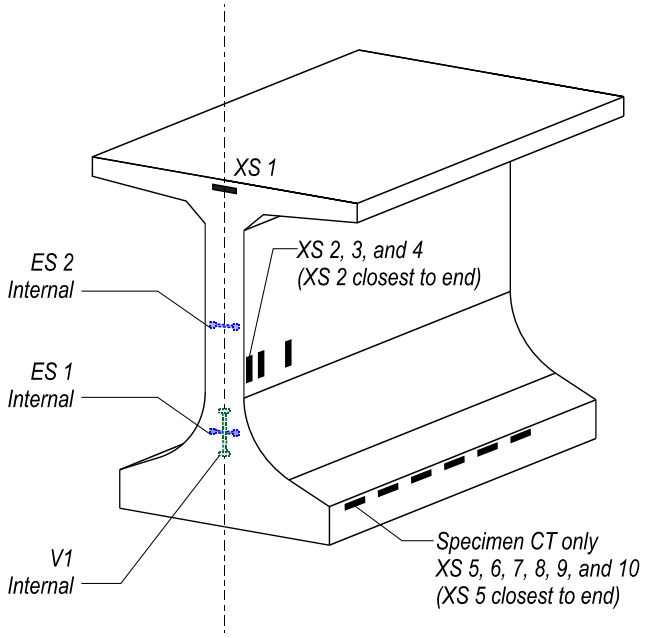

Figure 46–Gages at FIB-63 specimens

Strain gages placed on the concrete surface near the vibrating wire gage reported a similar magnitude of strain as the rods were post-tensioned (Figure 47). At the end of post-tensioning the vertical compressive strain at the end of the web was approximately 210 microstrain. Multiplying the experimental strains by an assumed a modulus of elasticity of 4750 ksi (based on measured compressive strength and empirical ACI equations) results in the stress profile shown in Figure 48. The location of zero stress at 17 in. was selected such that integrating the stress profile through the web results in 79kip which is close to the estimated post-tension force. This approximation is based on limited data, but does suggest that the post-tensioning was most significant at the end of the member and was effective over a finite distance of approximately 17 in. from the end.

Gage XS1 was placed horizontally at the end of the specimen near the post-tension bearing plate. This gage reported tension due to bursting action from the post-tension force. Although tensile strains were reported, no cracks were observed during or immediately after post-tensioning. Based on the experimental strain data it is estimated that the tensile strain at XS1 was approximately 585 psi at the end of post-tensioning.

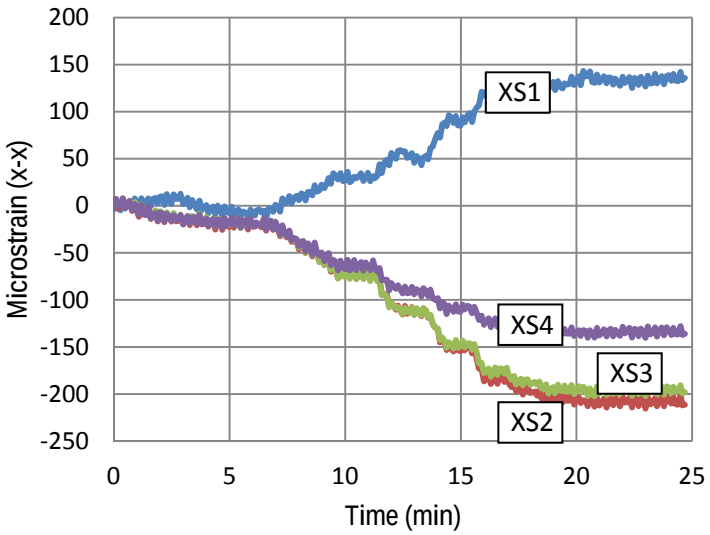

Figure 47–Strain due to post-tensioning process in XS gages

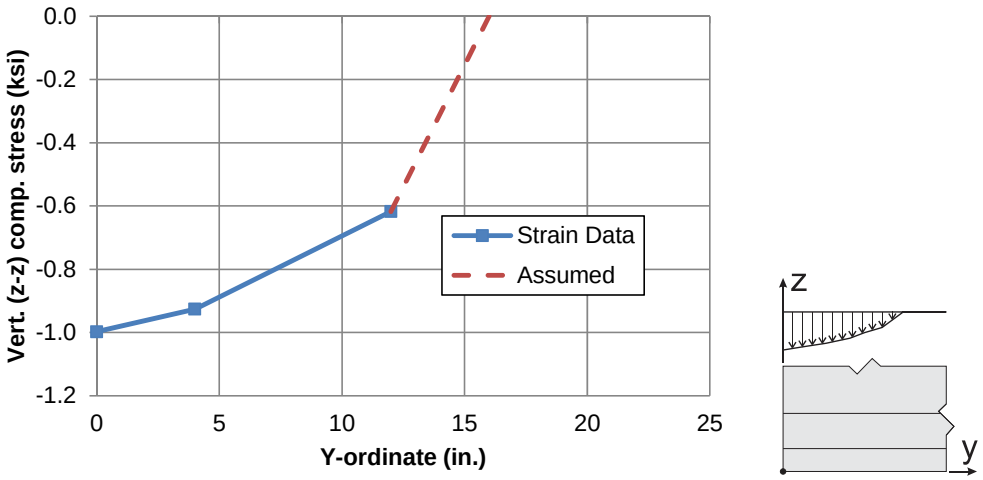

Figure 48–Estimated stress profile in web due to post-tensioning (tension positive)

5.2 Strain and Cracking during Prestress Transfer

Strain and crack data were collected during prestress transfer. To facilitate discussion of strain data, strand cutting events were broken into the stages listed in Table 15. Strand cutting events listed in Table 15 are keyed to the strand cutting pattern shown in Figure 49.

Table 15–Girder fabrication stages

Stage	Event
J	strands 1-4 cut
K	strands 5-30 cut
L	Pause
M	strands 30-56 cut
N	all strands cut

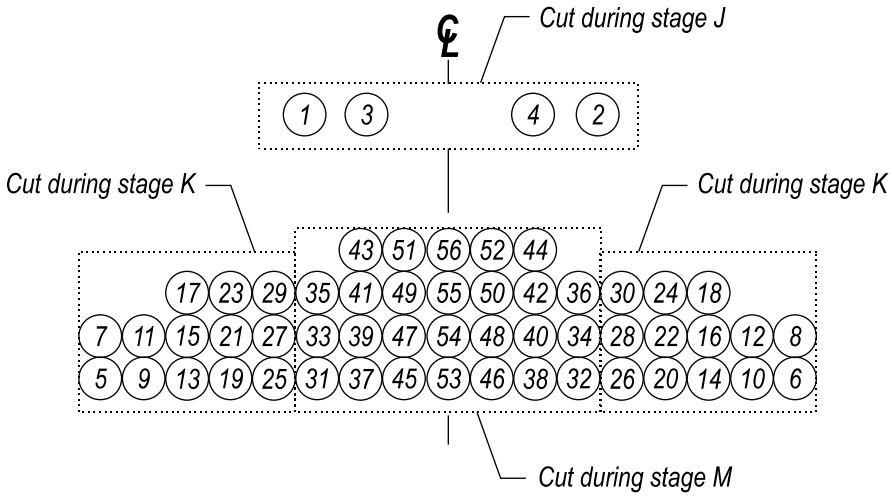

Figure 49–Strand cutting pattern groups

Vertical strain in the web became increasingly tensile in each specimen as prestress force was transferred to the girders (Figure 50 through Figure 53). Data indicate that strain was typically largest at the end of the girder (XS2) and smaller away from the end (XS4). For example, vertical strain in specimens CT at gage XS2 was 190 microstrain during stage L and only 90 microstrain at XS4.

Cracks were visually observed in specimen CT immediately after prestress transfer (Figure 54). Abrupt changes in strain behavior at approximately 57 minutes suggest that the cracks formed during stage M (Figure 50).

Cracks were also observed immediately after transfer in specimen LB (Figure 54). As with specimen CT, abrupt changes in strain behavior at approximately 57 minutes suggest that

the cracks formed during stage M (Figure 53). Cracking may have initiated during stage K as suggested by the abrupt changes at approximately 18 min.

Cracks were not observed in specimens SL or PT during or immediately after prestress transfer. The lack of cracking in these specimens is consistent with strain behavior demonstrated by the vertical gages. With the exception of XS2 on specimen SL, no abrupt changes in strain were observed in SL or PT. Lack of cracking in SL is attributed to the lower stresses affected by strand shielding. Lack of cracking in PT is attributed to the pre-compression in the web introduced by the post-tensioning.

For specimen PT, vertical strain at the beginning of transfer was initially compressive (Figure 52) due to the post-tension force discussed in the previous section. Strain reported by gages XS2 and XS3 became tensile as the outer strands were cut during stage M. Multiplying the final strain during stage N by an elastic modulus of 4750 ksi gives an estimated stress profile in the web (Figure 55). Integrating the tensile stress portion over the web area results in an estimated net tension force of 9.2kip.

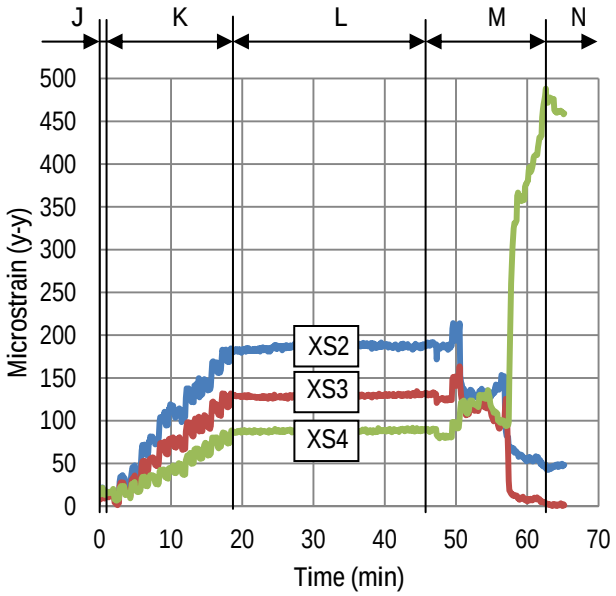

Figure 50–Concrete strain in specimen CT during prestress transfer

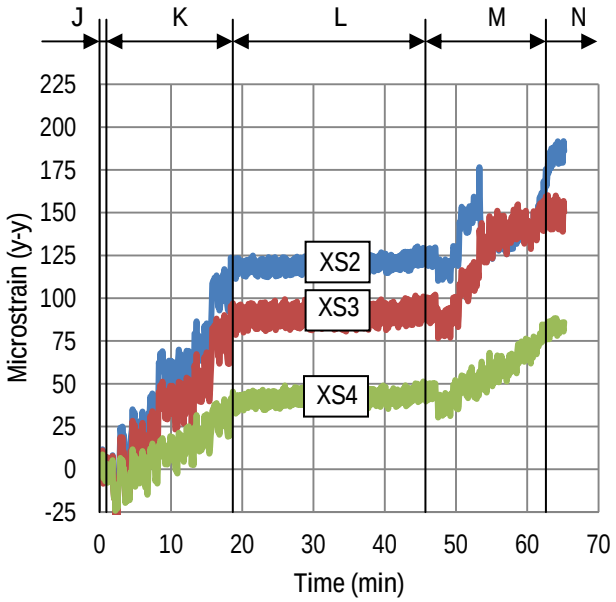

Figure 51–Concrete strain in specimen SL during prestress transfer

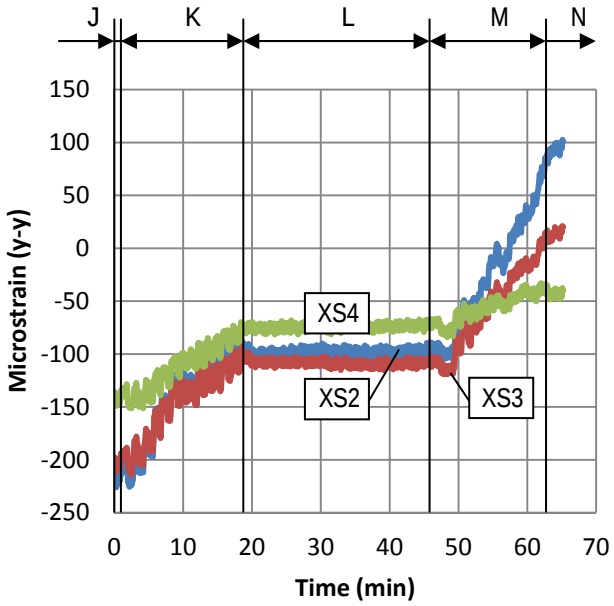

Figure 52–Concrete strain in specimen PT during prestress transfer

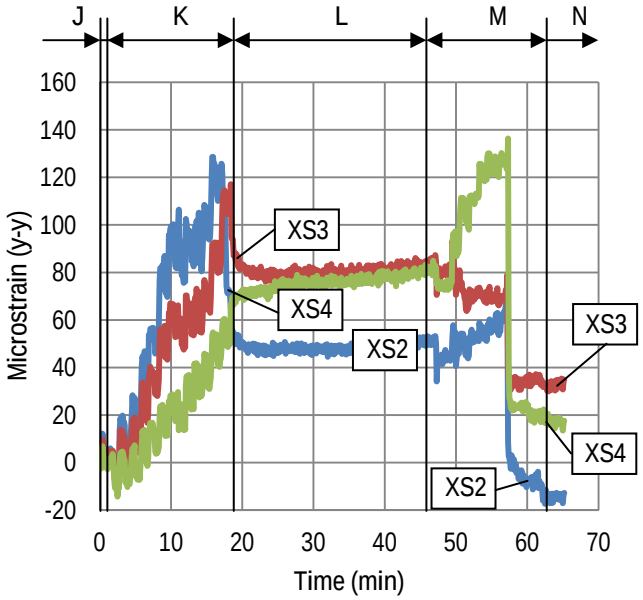

Figure 53–Concrete strain in specimen LB during prestress transfer

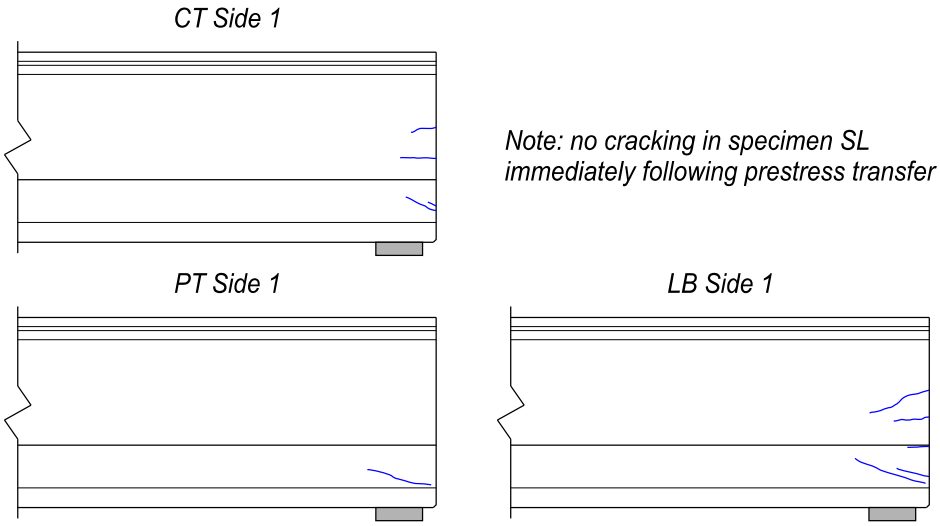

Figure 54–Cracks after prestress transfer

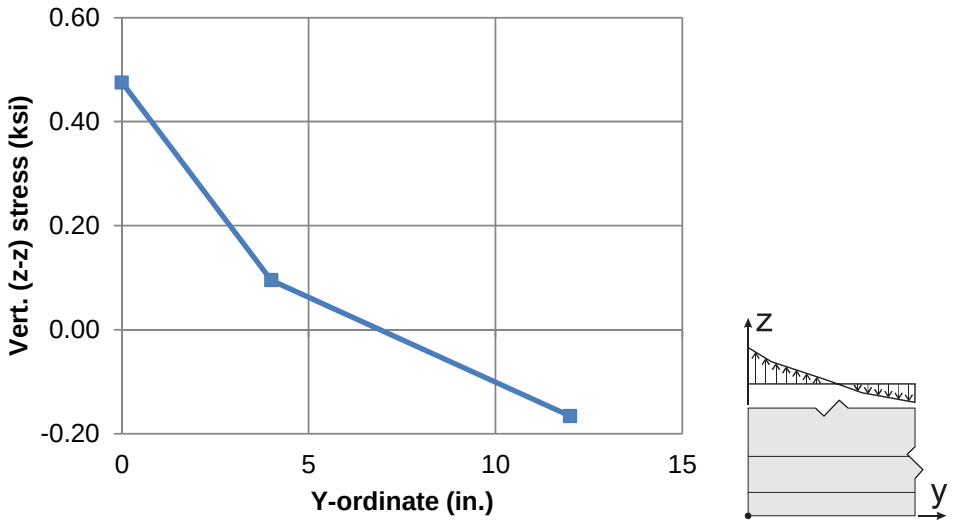

Figure 55–Estimated stress profile in web of specimen PT after transfer (tension positive)

Strain gages XS5 through XS10 (Figure 46) were placed on the bottom flange of CT to experimentally evaluate the transfer length. When sufficient data are available, the 95% Average Maximum Strain (AMS) Method is a well-established method for determining transfer length from experimental strain data (Russell and Burns 1996). The available strain data in the current study were insufficient to apply the AMS method, but were still sufficient to give an estimate of transfer length.

Strain data from stage N (all strands cut) are shown in Figure 56 for gages XS5 through XS10. Blue diamond markers indicate values from the gages. A bilinear curve representing the apparent strain is also shown. Gages reported increasing strain with increased distance from the girder end. The rate of increase dropped after 30 in. suggesting the end of the transfer length. A 30 in. estimated transfer length is consistent data from the FIB-54 girders fabricated at the same time (see Appendix D).

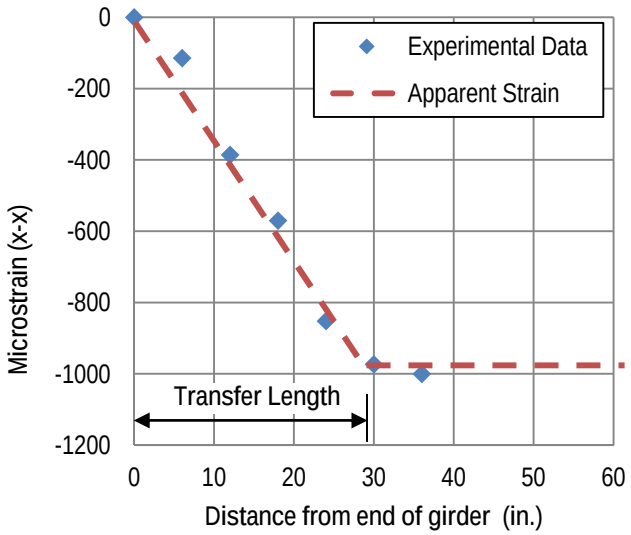

Figure 56–Strain and subsequent apparent transfer length

5.3 Web Cracks

Specimens were inspected for cracking during prestress transfer and during the days and weeks following transfer (Table 8). Cracks were first observed to form during prestress transfer. The initial cracks grew and additional cracks formed during the days and weeks following prestress transfer. Figure 57 shows the formation and propagation of cracking in specimen CT. Crack quantity and length also grew over time in the other specimens. Figures documenting cracking in the other specimens are included in Appendix H.

The observed crack patterns varied among specimens as shown in the photos in Figure 58. Cracks in the end region were observed in the top flange, web and bottom flange. Flexural cracks were also observed throughout the span lengths but are not shown in the figures. Cracks in each specimen prior to load testing are shown in Figure 59 through Figure 62. Web splitting cracks are the primary focus of the FIB-63 test program and are discussed in the proceeding paragraphs.

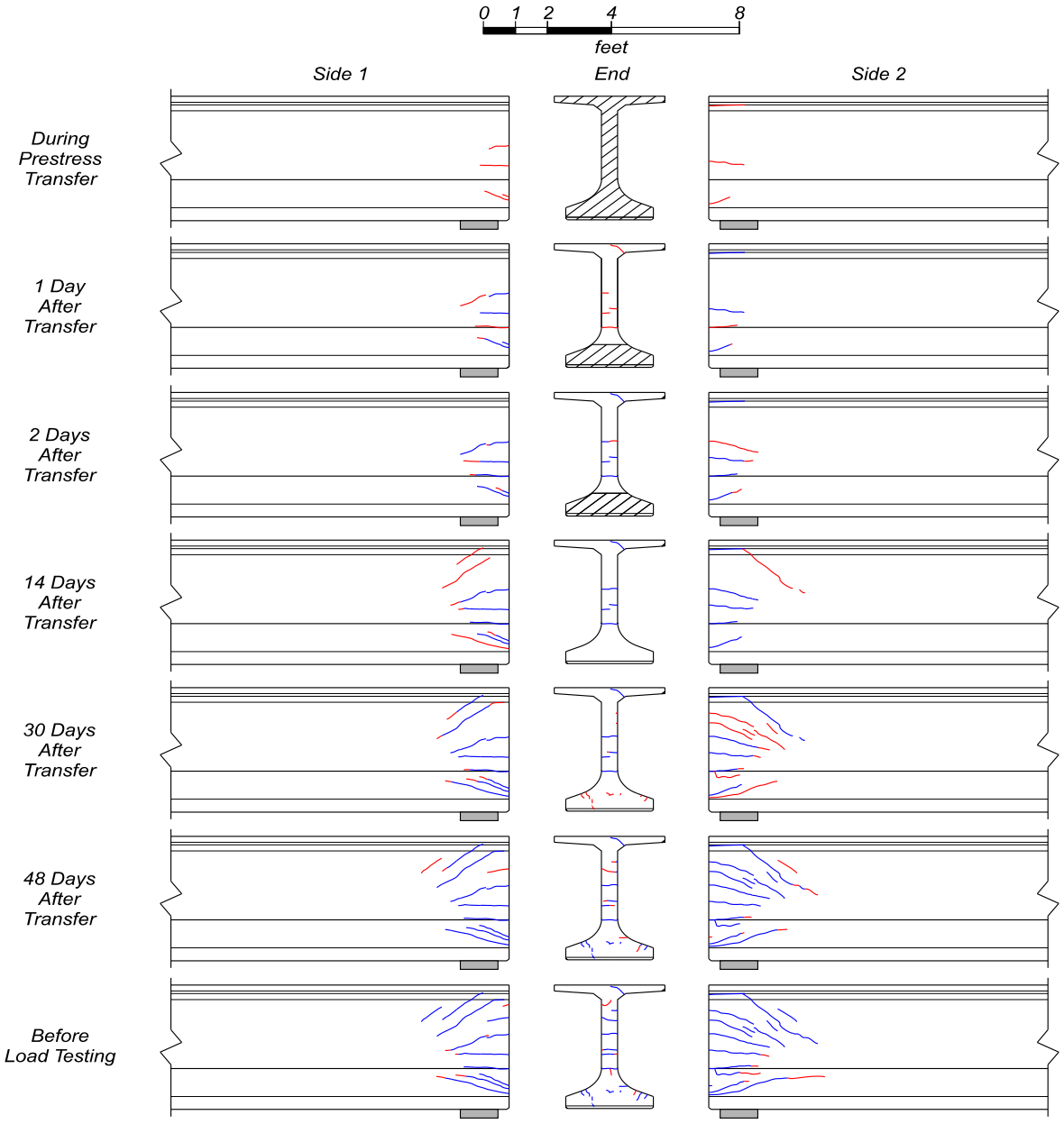

Figure 57–Crack growth in specimen CT (flexural cracks in top flange not shown)

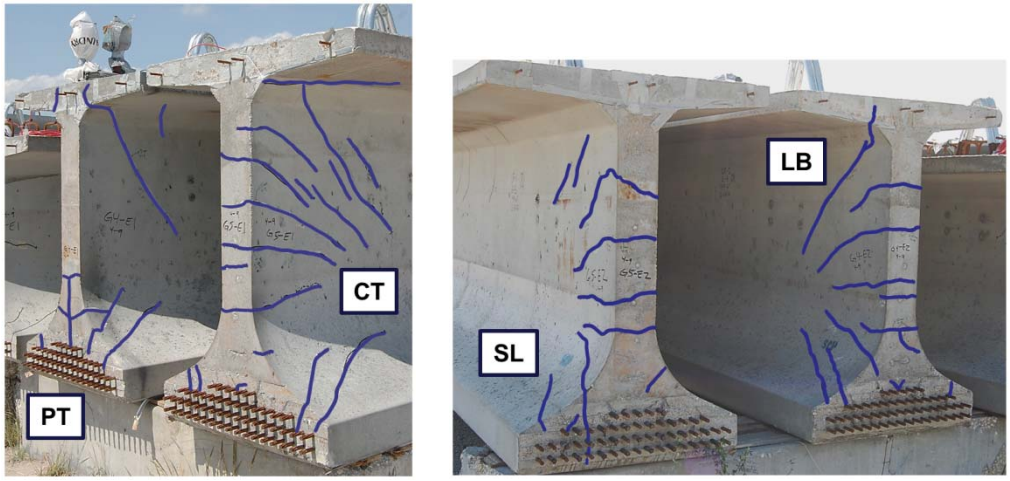

Figure 58–Photo of end region cracks (cracks enhanced in blue)

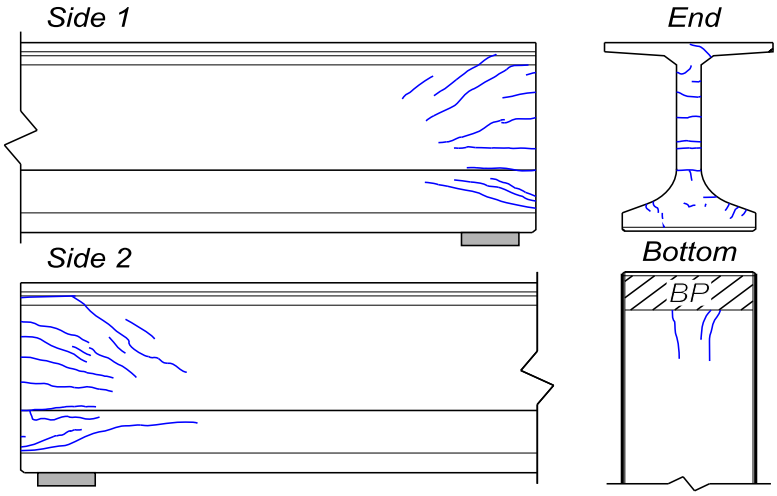

Figure 59–Specimen CT end region cracks prior to load testing

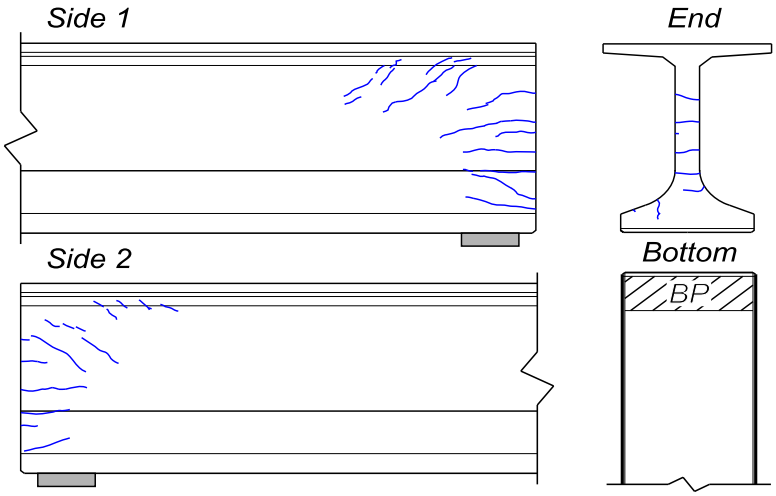

Figure 60–Specimen SL end region cracks prior to load testing

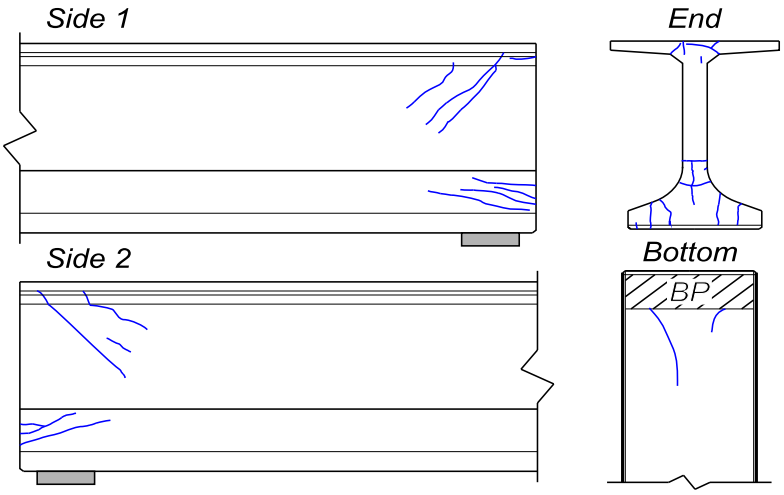

Figure 61–Specimen PT end region cracks prior to load testing

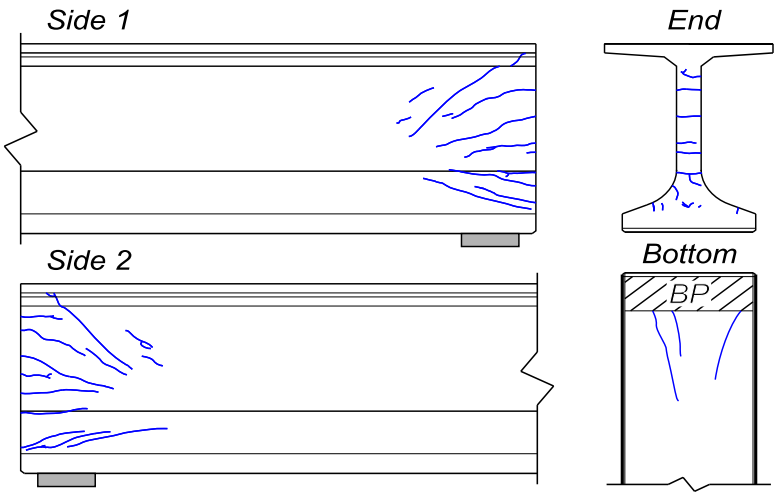

Figure 62–Specimen LB end region cracks prior to load testing

Web crack data from each specimen are quantified in Figure 65 and Figure 66. Four metrics are used for comparison: total length, total area, average width and maximum width. Total length was calculated by the summing the length of all individual web cracks in a specimen. Total area is the summation of areas from the individual web cracks, which was calculated by multiplying the individual crack lengths by a representative width. Average width was calculated by dividing the total area by the total length. Finally, maximum crack width was taken as the maximum width observed by the microscope readings.

Representative widths used to calculate crack area were derived from width measurements taken by microscope. The means of determining the representative width was different depending on the crack location. For the portion of a crack on the end face of a specimen, the representative width was taken as the measured width (Figure 63). Where multiple measurements were taken for the same crack on the end face, the representative width was taken as the average of the measurements. For the portion of a crack on the side of a specimen (Figure 64) the representative width was taken as the average of all widths measured along the crack. Only a single measurement was taken for some cracks on the specimen sides. The single measurements typically occurred near the end face where cracks had their greatest width. In these cases, the representative width was taken as one-half of the measured width.

Figure 63–Web crack measurements (view from end of specimen)

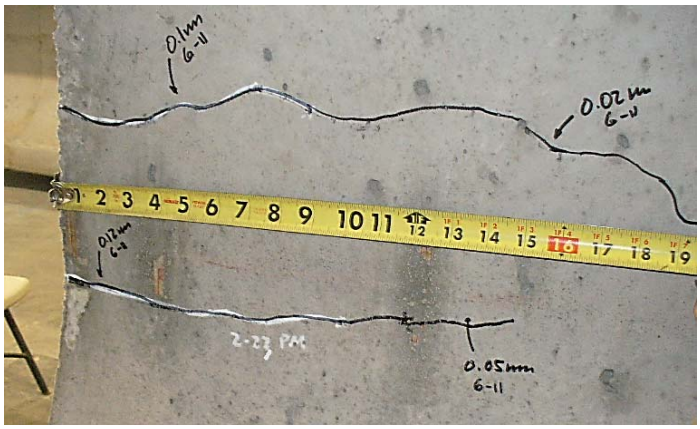

Figure 64–Web crack measurements (view from side of specimen)

Some degree of cracking is expected and generally accepted in the end region of pretensioned girders. Tadros et al. (2010) presented criteria for evaluating crack widths and determining when web cracks should be repaired (Table 16). According to these criteria, web splitting cracks wider than 0.012 in. require corrective action. Cracks with widths less than 0.012 in., though undesirable, do not warrant corrective action. Web crack widths in this test program were less than 0.012 in. and would not require corrective action according to the Tadros et al. criteria. FDOT specifications contain similar repair criteria, requiring corrective action for web cracks greater than 0.012-in. wide (FDOT 2011). For girders used in environments characterized as extremely aggressive, FDOT specifications requires corrective action for all web splitting cracks regardless of width.

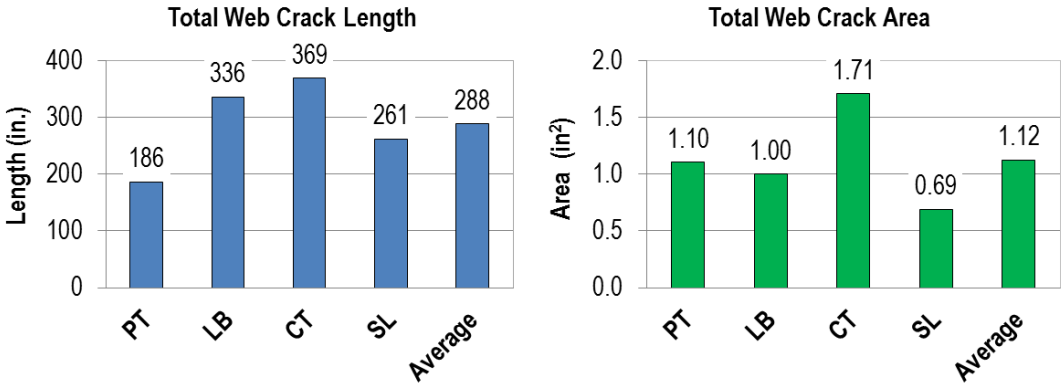

Figure 65–Web splitting crack length and area

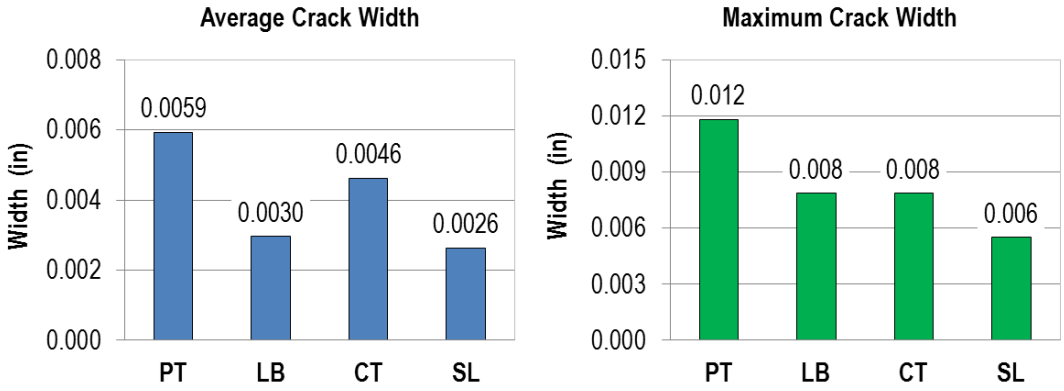

Figure 66–Web splitting crack widths

Table 16–Recommend action for web splitting cracks (Tadros et al. 2010)

Crack Width (in.)	Required Action
Less than 0.012	None
0.012 to 0.025	Fill cracks with cementitious material and apply surface sealant to end 4 ft of girder
0.025 to 0.05	Fill cracks with epoxy and apply surface sealant to end 4 ft of girder
Greater than 0.05	Reject girder unless shown by detailed analysis that structural capacity and long-term durability are sufficient

Data presented in Figure 65 and Figure 66 are useful for comparing the relative effectiveness of the different detailing schemes in controlling web cracks. Based on the metrics of total length and total area, the control detail (specimen CT) was the least effective in

controlling web splitting cracks. Specimen CT at had 28% more length and 53% greater area than the average of all specimens.

Specimen SL was the most effective detail according each metric except total length. SL had 59% less area, and 44% smaller average width than the control specimen. The reduction in crack length, area, and width observed in specimen SL is attributed to the partial strand debonding which reduced tensile stresses in the end region.

In terms of crack length, the post-tensioning detail of specimen PT was the most effective for controlling web splitting cracks. Web splitting crack length in specimen PT was 50% less than the control specimen. Figure 61 shows that the post-tensioning effectively mitigated all web cracks at the end surface of the member. Web cracking did, however, occur away from the end surface.

Web cracks away from the end of specimen PT extended diagonally into the web from the post-tensioning anchor plate. Forces introduced at the plate are believed to have contributed to the formation of the diagonal cracking in specimen PT. The diagonal web crack in PT had the greatest width of web crack in the test program. Specimen PT also had the largest average web crack width of approximately 0.006 in. This value was 30% greater than the control specimen.

Detailing of specimen PT had negative effect on the bottom flange spitting cracks. Referring to Figure 61, it can be observed that PT was the only specimen to have a vertical splitting crack on the end surface. This crack is attributed to development of the post-tensioning rods in the bottom flange.

Specimen LB compares well against the control specimen in every metric except maximum crack width, for which LB and CT both had a maximum crack width of 0.008 in. For LB, the total web crack length was 10% smaller and the average web crack width 35% smaller, than in the control specimen.

5.4 Prestress Losses

Vibrating wire strain gages were placed longitudinally near mid span to experimentally evaluate prestress losses. The gage in the girder PT/LB malfunctioned before valid data could be collected. The gage in girder CT/SL also malfunctioned, but not before sufficient data were collected to evaluate elastic losses. Experimental and code-calculated prestress losses are presented in Table 17.

Experimentally determined elastic loss in the girder with specimens CT and SL was higher than the AASHTO and PCI calculated elastic losses. The experimental long term losses, however, were less than half of those calculated by the code methods. This is likely due to the fact that the experimental long term losses were not actually long term; they were taken over a two week period. The AASHTO and PCI long term losses assume a much longer time period. Based on the experimental results it is believed that total losses were approximately 30% at the time of load testing. FIB-54 girders fabricated at the same time the FIB-63 specimens reported 12%-17% elastic losses and 22%-30% total losses (see appendix D).

Table 17–Experimental and code prestress losses

Prestress Losses	Experimental		Code	
	CT and SL*	PT and LB**	AASHTO	PCI
Elastic Losses (%)	18.9%	N/A	15.1%	11.8%
Long Term Losses (%)	9.2%	N/A	15.0%	26.9%
Total Losses (%)	28.2%	N/A	30.1%	38.7%
Measurement Period (Days)	14	-	-	-
Initial Prestress (kip)	2354			

* Gage malfunction at 14 days

** Gage malfunction

5.5 Load Tests

Load tests were conducted to evaluate the effects of each detailing scheme on end region capacity. Specimens were loaded in 3-point bending and an a/d ratio of approximately 2. Test results are presented in terms of superimposed shear, which is defined as the shear due to the applied load at the near support. Self-weight is not included in the superimposed shear. Displacement results are presented as the vertical displacement at the load point. Results have been adjusted to remove the effects of bearing pad displacement.

Each specimen was loaded twice. The first test mimicked service loading and the second test determined ultimate capacity. Maximum shear force in the service load test was 390kip. Shear-displacement data from the ultimate load tests are presented in Figure 67, and shear-strand slip date are presented in Figure 68. Slip data is presented as the average slip of all monitored fully bonded strands. Specimen LB was excluded from Figure 68 due to minimal slip.

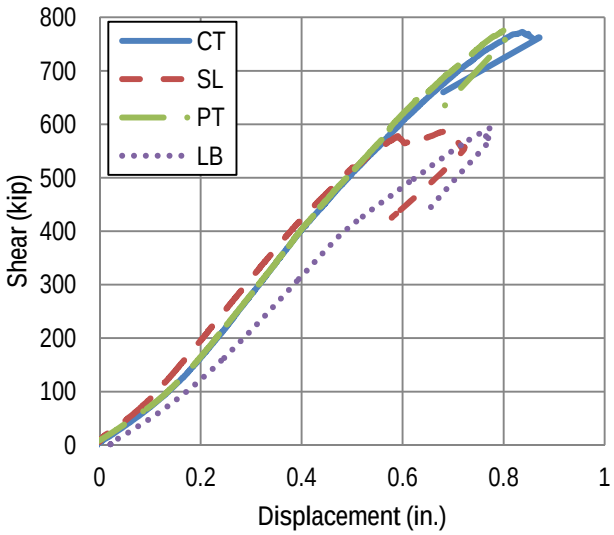

Figure 67–Ultimate load test shear-displacement for all specimens

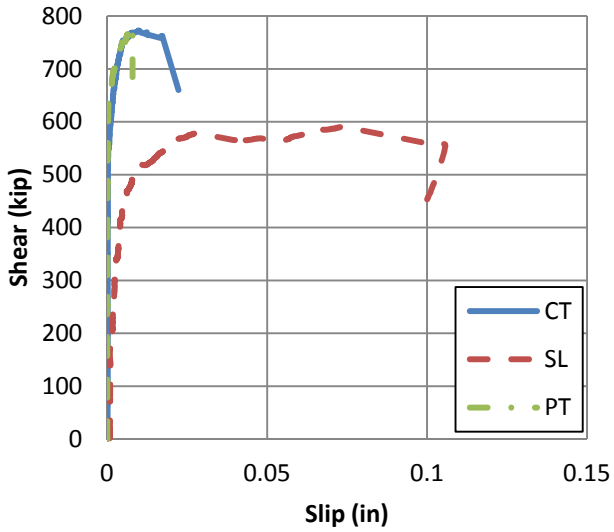

Figure 68–Ultimate load test shear-strand slip for specimens CT, SL, and PT

Shear forces associated with the first cracks during load testing are listed in Table 18. In three of the four specimens cracking was first reported by strain gage placed diagonally on the web (Figure 69) within the shear span. The first crack in each specimen was an inclined crack in the web. Discussions of load, slip, and crack data are presented in the following sections for each of the four specimens.

Table 18–First cracks during service load testing

Specimen	Shear at first crack observation	
	Gage (kip)	Visual (kip)
CT	350	345
SL	240	275
PT	350	370
LB	310	365

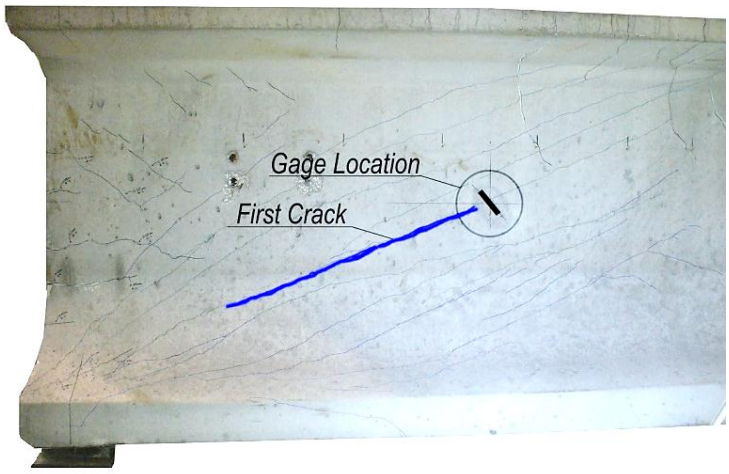

Figure 69–Strain gage and typical first crack location

5.5.1 CT

Vertical reinforcement in the end region of specimen CT (Figure 9) was based on FDOT standards. All (52) strands in specimen CT were fully bonded (Figure 7).

Load-displacement response of CT was approximately linear-elastic during service and ultimate loading (Figure 67). The first crack to form during the service load test occurred in the web at a superimposed shear of 350 kip. Additional web cracks formed at higher loads during the service and ultimate strength tests. Flexural cracks were not observed.

Strand slip in CT was negligible until the superimposed shear reached approximately 550 kip. Slip increased gradually beyond 550 kip, reaching a maximum slip of 0.016 in. at peak load.

Specimen CT failed in a brittle manner at a shear force of 773 kip. At this load the web crushed in dramatic fashion with concrete pieces spalling off the girder. Failure was categorized as a web-shear shear failure (Figure 70). After testing it was observed that the top hooks of the vertical reinforcement experienced breakout failure due to lack of sufficient cover (Figure 71). Top hooks from the vertical reinforcement were embedded in the relatively thin top

flange because a topping slab was not cast on the specimen. It is not known if the hook failure precipitated or was a by-product of the web failure. The bearing pad at the load point also punched through the top flange at peak load (Figure 71).

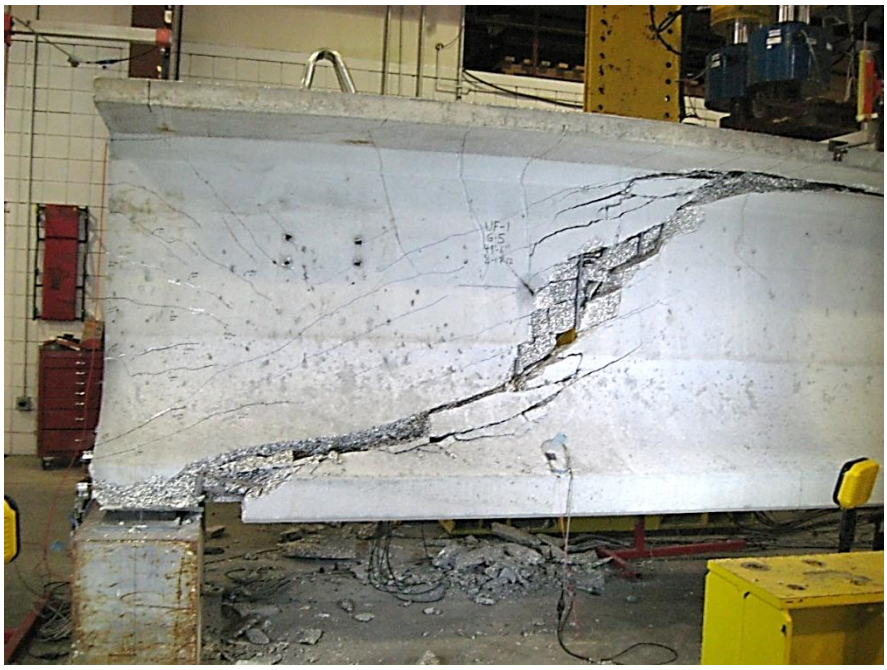

Figure 70–Specimen CT after load tests

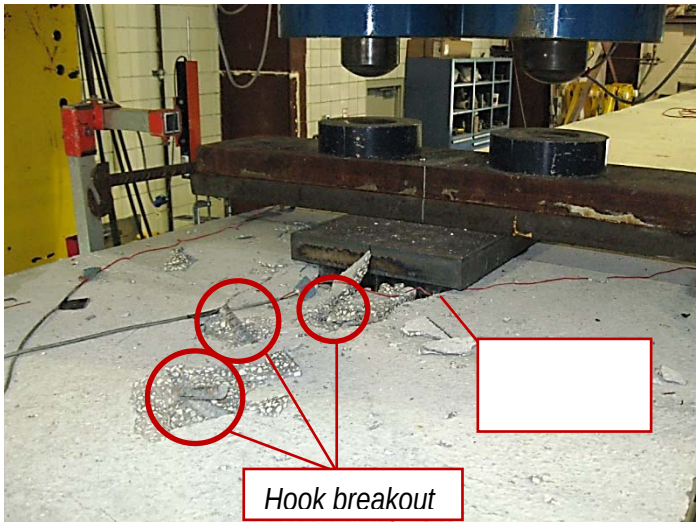

Figure 71– Punching failure and hook breakout at load point

5.5.2 SL

Vertical reinforcement in specimen SL (Figure 9) was based on FDOT standards. Of the (52) strands in SL, (23) were shielded for 5 ft from the specimen end (Figure 7).

Load-displacement response of SL was approximately linear-elastic during service load test and during the initial portion of the ultimate loading (Figure 67). The first crack to form during the service load test occurred in the web at a superimposed shear of 240 kip. Load at first crack was 30% to 45% lower than the other specimens. The lower cracking load is attributed to the reduced prestress force occurring at the end of specimen SL. This result demonstrates a potential serviceability problem with strand shielding. Although shielding reduces the vertical tensile stresses leading to web splitting cracks at prestress transfer, shielding also reduces the horizontal compressive stresses that acts to delay cracks in the web due to loading. Flexural cracks were not observed.

Additional cracks formed as the load increased beyond the initial cracking load. Some of these cracks entered the bottom flange thereby interrupting strand development and affecting strand slip. Popping sounds indicative of strand slipping were heard beginning at shear of approximately 390kip. Based on the shear-slip behavior shown in Figure 68 it is believed that strand slip started at approximately 300kip. Strands in SL began slipping at lower loads and slipped a greater distance than did strands in the other specimens. Peak load in SL corresponded to a strand slip event. As such, failure of SL was categorized as a bond-shear failure (Figure 72, Figure 73).

Specimen SL supported a maximum shear of 591kip, which was the smallest peak load of all the test specimens. The reduced number of fully bonded strands in SL was culpable for the bond-shear failure and lower capacity. Specimens CT, LB, and PT had almost twice as many bonded strands and were less affected by cracks interrupting the strand development length. As such bond-shear failure did not occur in these other specimens.

After reaching the maximum load, SL continued to carry load with a stick-slip behavior controlled by strand slip. Load was removed after it had become apparent from the load-displacement curve that peak load had been reached. Because of the stick-slip behavior, failure of SL was slightly more ductile than the other specimens (Figure 67).

Figure 72–Bond shear failure of specimen SL

Figure 73–Bottom flange cracking at SL bearing.

5.5.3 PT

The end of specimen PT (Figure 10) was vertically post-tensioned by tightening threaded rods prior to prestress transfer. PT also had a 33% reduction in vertical end region reinforcement relative to specimen CT. All of the (52) strands in PT were fully bonded (Figure 7).

Shear-displacement response of PT was approximately linear-elastic throughout the service and ultimate load tests (Figure 67). The first crack to form during the service load test occurred in the web at a superimposed shear of 350 kip. Additional web cracks formed at higher loads during the service and ultimate strength tests. Flexural cracks were not observed.

Strand slip behavior in specimen PT was similar to the control specimen (Figure 68). This result suggests that the vertical post-tensioning did not influence the strand-concrete bond

during ultimate load testing. Maximum slip in PT was approximately 0.01 in. occurring at peak load.

Specimen PT did not fail before reaching the capacity of the test apparatus and failure behavior could not be determined. Specimen PT was loaded to 782kip in shear, which was the greatest of any specimen. This result suggests that the post-tensioning had no adverse effect on the ultimate capacity. Multiple web cracks had formed in the web prior to peak load (Figure 74). Some of these cracks had propagated to the end of the specimen.

Figure 74–Cracking specimen PT

5.5.4 LB

Vertical end zone reinforcement in specimen LB (Figure 10) consisted of eight 1-in. diameter vertical threaded rods. These rods represented a 30% increase in vertical end region reinforcement relative to the control specimen CT. Each of the (52) strands in specimen LB was fully bonded (Figure 7).

Load-displacement behavior of LB was approximately linear-elastic throughout the ultimate load test (Figure 67). Apparent stiffness of LB was less than the other specimens. This difference is attributed to the orientation of the load point (Figure 30). Because the applied load was spread directly to the outer portions of the top flange, it is believed that the flange in specimen SL experienced a greater degree of displacement. The LVDTs monitoring vertical displacement (Figure 40, Figure 75) were placed at the edges of the flange and would have been sensitive to differences in displacement resulting from the load condition unique to LB.

Additional displacement due to the load condition affects the lower stiffness of LB relative to the other specimens.

The first crack to form during the service load test occurred in the web at a superimposed shear of 310 kip. Additional web cracks formed at higher loads during the service and ultimate strength tests. Flexural cracks were not observed.

Specimen LB failed in the top flange due to punching failure (Figure 75). Punching failure occurred because load was applied across the width of the relatively thin top flange. Cracking associated with punching failure is shown in the photos in Figure 76 and Figure 77.

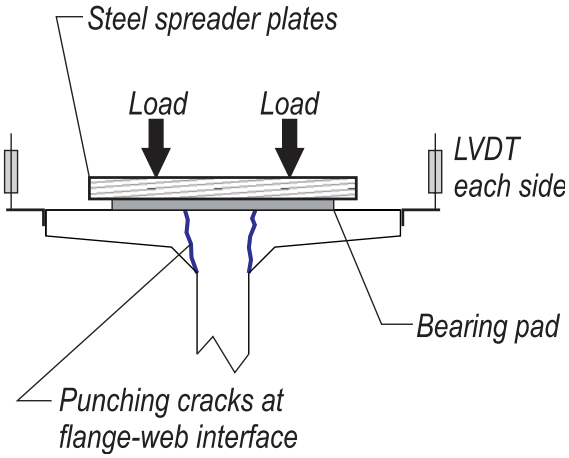

Figure 75–Punching failure specimen LB

Strand slip in specimen LB was negligible. Lack of slip was due to the relatively low loads supported by LB. Had LB supported similar loads to CT and PT, strand slip likely would have occurred.

Specimen LB supported a maximum shear of 594kip. Specimen LB was the first to be load tested. To prevent the reoccurrence of punching shear failure in the other specimens the load point configuration was adjusted.

Figure 76–Punching shear failure in specimen SL

Figure 77–Punching failure from above (left) and below (right)

5.6 Code Comparison

Experimental shear capacities were compared to nominal capacities calculated from three different procedures:

- Detailed procedure from ACI 318. (labeled as ACI Vn)
- General procedure from AASHTO LRFD. (labeled as LRFD Vn)
- End region tie requirement based on AASHTO LRFD 5.8.3.5. (labeled as Tie Vn)

All calculated capacities were based on the tested material properties and losses. Calculations of the end region tie requirement followed the procedure proposed by Ross et al. (2011) for determining a nominal capacity based on AASHTO LRFD minimum tie requirements. A required development length 60 in. was assumed and an available development length of 25

in. was assumed. The nominal capacity due to the end region tension tie was lower for SL than for the other specimens because SL had fewer fully bonded strands to act as a tension tie.

The critical section for nominal shear capacity calculations (ACI and LRFD) occurred at the load point. At this section the prestressing force, reinforcement, and material properties where the same for each specimen, and all specimens have the same ACI and LRFD nominal capacities.

Nominal capacities from each method are presented in Table 19 along with maximum experimental shear forces. To facilitate comparison with nominal capacities, the maximum experimental shear forces listed in the table include the superimposed shear and the self-weight shear.

When comparing experimental and nominal capacities it is critical the failure behavior of the specimens be considered. Specimens CT failed in web-shear and can be directly compared to the ACI and LRFD nominal capacities which are based in-part on web-shear failure. Specimen SL failed in bond-shear and can be directly compared to the nominal capacity from the tie requirements which were derived assuming bond-shear failure. Specimen PT did not fail during testing and cannot be directly compared with any of the methods. Finally, specimen LB failed in flange punching shear which is not considered by any of the calculation methods.

Table 19–Code comparison with experimental shear forces

Specimen	V_{exp} (kip)	ACI V_n (kip)	LRFD V_n (kip)	Tie V_n (kip)	EXP / ACI	EXP / LRFD	EXP / TIE
CT	791	524	516	997	1.51	1.53	0.79
SL	609	524	516	673	1.16	1.18	0.90
PT	800	524	516	997	1.53	1.55	0.80
LB	612	524	516	997	1.17	1.19	0.61
Average					1.34	1.36	0.78

Important information can be gleaned from the comparisons in Table 19 in spite of the different failure modes exhibited by the specimens and assumed in the calculation procedures. First, the experimental capacities were always greater than nominal shear capacities calculated by ACI and LRFD. Thus the ACI and LRFD methods were conservative relative to the test results, regardless of failure behavior. Second, the experimental capacity of specimen SL was 10% lower than the nominal capacity based on the end region tie. It is critical to select

appropriate values for the available and required strand embedment as these the nominal tie capacity is sensitive to these values. Calculations for SL assumed 60 in. and 25 in. for the required and available strand embedment and these values appear to be slightly unconservative relative to the experimental results. LRFD section 5.8.3.5 which governs the end region tie requirements does not give explicit instructions regarding the available and required development to be used. Rather the LRFD says that "and lack of full development shall be accounted for."

6 Summary and Conclusions

Four FIB-63 test specimens were fabricated and load tested to evaluate the effects of different end region detailing schemes on the control of web splitting cracks. Details in the test program included: 1) #5 vertical end region reinforcement per current FDOT standards (control specimen), 2) vertical reinforcement per FDOT and 45% partial strand shielding, 3) vertical end region post-tensioning, and 4) 1-in. diameter threaded rods as vertical reinforcement. Cracks and strains were monitored during prestress transfer and in the days and weeks following transfer. These data were used to compare the relative effectiveness of each detailing scheme in controlling web splitting cracks. Finally, specimens were load-tested in 3-point bending to determine what, if any, effect the end region detailing had on shear capacity and behavior. Key observations and conclusions are as follows:

- Partial strand shielding was an effective means of controlling the length, and width of web splitting cracks. Of the 52 strands in specimen SL 45% were shielded within the end region. Shielding resulted in a 29% reduction in web crack length and a 43% reduction in average web crack width relative to the control specimen.
- Vertical post-tensioning of specimen PT prevented web splitting cracks at the end surface, but affected other web cracks away from the end and in the bottom flange. The largest web cracks in the test program occurred in specimen PT.
- All web cracks in the test program had widths equal to or less than 0.012 in. Cracks above this width require corrective action based on FDOT requirements for moderate environments.
- Increasing the end region vertical reinforcement decreased the length and width of web splitting cracks. Specimen LB had 30% more vertical end region reinforcement than the control specimen, and had 10% less web crack length and 35% lower average web crack width.
- Experimental capacity of all specimens was greater than the ACI and LRFD calculated nominal shear capacities.

- Increased strand shielding in specimen SL resulted in a reduction in the experimental capacity of specimen SL. Because of strand shielding this specimen had insufficient fully bonded strands to prevent bond-shear failure after cracks formed in the above flange in front of the bearing.
- Vertical post-tensioning in the end region of specimen PT did not affect load capacity. Specimen PT supported the largest load of any specimen. Failure of PT could not be reached due to limitations of the testing equipment.
- Specimen LB experienced a punching shear failure in the top flange due to placement of the applied load. Consequently, the effect on load capacity of increased vertical reinforcement (relative to the control) in specimen LB could not be evaluated. It is assumed that the additional vertical reinforcement would not have had negative effect.
- During load testing, inclined cracking in specimen SL initiated at a load 30% to 45% lower than in the other specimens. The lower cracking load in SL occurred due to decreased end region compressive stresses affected by strand shielding.